



OPEN

SUBJECT AREAS:
NEUROSCIENCE
COGNITIVE NEUROSCIENCEReceived
22 August 2014Accepted
3 December 2014Published
6 January 2015Correspondence and
requests for materials
should be addressed to
G.G. (guy.griebel@
sanofi.com)

Selective blockade of the hydrolysis of the endocannabinoid 2-arachidonoylglycerol impairs learning and memory performance while producing antinociceptive activity in rodents

Guy Griebel¹, Philippe Pichat¹, Sandra Beeské¹, Thibaud Leroy¹, Nicolas Redon¹, Agnès Jacquet¹, Dominique Françon¹, Lionel Bert², Luc Even¹, Mati Lopez-Grancha³, Tatiana Tolstykh⁴, Fangxian Sun⁴, Qunyan Yu⁴, Scott Brittain⁴, Heike Arlt⁴, Timothy He⁴, Bailin Zhang⁴, Dmitri Wiederschain⁴, Thomas Bertrand⁵, Jacques Houtmann⁵, Alexey Rak⁵, François Vallée⁵, Nadine Michot⁵, Franck Augé¹, Véronique Meneré⁶, Olivier E. Bergis¹, Pascal George³, Patrick Avenet¹, Vincent Mikol⁵, Michel Didier² & Johanna Escoubet²

¹Sanofi R&D, Exploratory Unit, Chilly-Mazarin, France, ²Exploratory Unit, Montpellier, France, ³Therapeutic Strategic Unit Aging, Chilly-Mazarin, France, ⁴Global Oncology Division, Cambridge, USA, ⁵Lead Generation To Candidate Realization, Vitry-sur-Seine, France, ⁶Therapeutic Strategic Unit Aging, Montpellier, France.

Monoacylglycerol lipase (MAGL) represents a primary degradation enzyme of the endogenous cannabinoid (eCB), 2-arachidonoylglycerol (2-AG). This study reports a potent covalent MAGL inhibitor, SAR127303. The compound behaves as a selective and competitive inhibitor of mouse and human MAGL, which potently elevates hippocampal levels of 2-AG in mice. *In vivo*, SAR127303 produces antinociceptive effects in assays of inflammatory and visceral pain. In addition, the drug alters learning performance in several assays related to episodic, working and spatial memory. Moreover, long term potentiation (LTP) of CA1 synaptic transmission and acetylcholine release in the hippocampus, two hallmarks of memory function, are both decreased by SAR127303. Although inactive in acute seizure tests, repeated administration of SAR127303 delays the acquisition and decreases kindled seizures in mice, indicating that the drug slows down epileptogenesis, a finding deserving further investigation to evaluate the potential of MAGL inhibitors as antiepileptics. However, the observation that 2-AG hydrolysis blockade alters learning and memory performance, suggests that such drugs may have limited value as therapeutic agents.

The endocannabinoid (eCB) system is formed by the G protein-coupled receptors, CB1 and CB2, and their main transmitters, 2-arachidonoylglycerol (2-AG) and N-arachidonoylethanolamine (anandamide; AEA)¹. eCBs play an important neuromodulatory role in the peripheral and central nervous system (CNS), modulating a wide range of physiological and pathological processes, including cognition, emotion, mood, appetite and pain². Alterations in the eCB system have been observed in a variety of diseases across therapeutic areas. For example, changes in tissue concentrations of AEA and 2-AG have been observed in pain and inflammation^{3,4}, immunological disorders⁵, neurological and psychiatric conditions⁶, obesity and metabolic syndromes^{7,8} and cancer⁹. These observations have fueled significant interest in the development of eCB-manipulating drugs to treat these conditions^{10–12}. For example, CB1 antagonism has been demonstrated to limit the risks of cardiovascular disease and type 2 diabetes^{13–17}, but also to produce a number of undesirable CNS side effects¹⁸. As of today the efforts to uncouple these beneficial and unwanted effects have not been successful, thus limiting the therapeutic value of direct CB1 receptors ligands.



Inhibition of 2-AG and AEA catabolism has been suggested to represent an alternative avenue to modulate the eCB system^{19–22}. The signaling functions of these two transmitters are terminated by enzyme hydrolysis in processes principally mediated by the serine hydrolases monoacylglycerol lipase (MAGL)²³ and fatty acid amide hydrolase (FAAH)²⁴, respectively. While FAAH inhibitors have been discovered, characterized in several animal models of disease and are in pharmaceutical development (for a recent review, see²⁵), MAGL inhibitors have lagged behind. However, they may offer certain advantages over FAAH inhibitors because of their greater eCB specificity^{19,26,27}.

Several compounds with selectivity for MAGL have been described (for reviews, see^{19,22,28}). For example, lead MAGL inhibitors from the O-aryl carbamate class, such as JZL184 and its analog KML29 show good selectivity (>100-fold) for MAGL over FAAH and most other serine hydrolases^{29,30}. However, JZL184 inhibits several carboxylesterase enzymes in peripheral tissues, has cross-activity with FAAH after repeated administration and appears to be less potent in inhibiting MAGL in rats when compared to mice^{31,32}. Moreover, all potent inhibitors of MAGL activity reported thus far are claimed irreversible because they produce their action by forming covalent bonds with reactive cysteine or serine residues. The only exception is the naturally occurring terpenoid, pristimerin, which inhibits MAGL activity with high potency through a reversible mechanism²⁸. The most extensively studied selective MAGL inhibitors are JZL184 and KML29. When administered in mice, both drugs dramatically decreased brain MAGL hydrolysis activity and concomitantly elevated 2-AG levels in the brain. These metabolic and biochemical modifications were accompanied by several CB1- or CB2-dependent behavioral effects, such as analgesia and anxiolysis^{30,33–38}. Importantly, while JZL184 elicited cannabimimetic untoward effects, including hypothermia, and hypomotility²⁹, KML29 was devoid of such effects³⁸.

Here, we report the detailed characterization of a structurally distinct carbamate compound that acts as a highly potent and selective MAGL inhibitor, here named SAR127303 (Figure 1). While our data confirm that MAGL inhibition translates into antinociceptive effects *in vivo*, we also provide new evidence that blockade of this enzyme affects cognitive processes and epileptogenesis.

Methods

Ethics statement. All experimental procedures described herein were carried out in accordance with the “Guide and Care and Use of Laboratory Animals” (National Institutes of Health) and approved by the Sanofi Institutional Animal Care and Use Committee (studies conducted in the USA) or the Animal Ethics Committee of Sanofi (studies conducted in France).

Animals. Animals had access to food and water ad libitum with a 12-h light/dark cycle (lights on at 7:00 a.m.). The following species and strains were used: (1) mice: C57BL/6j, CB17 SCID, CD1, NMRI, OF1 and Swiss; (2) Rats: Sprague-Dawley, Wistar and Wistar Han (see below for further details). All testing was performed during the light (day) cycle.

Drugs. SAR127303, diazepam, rimonabant, SR144528, WIN55,512-2 (Sanofi Medicinal Chemistry, France), levetiracetam (Advanced Technology & Industrial Co. Ltd, Hong Kong), kainic acid, pentylentetrazol and MK-801 (Sigma RBI, St Quentin Fallavier, France) were dissolved or suspended in distilled water with 0.6%

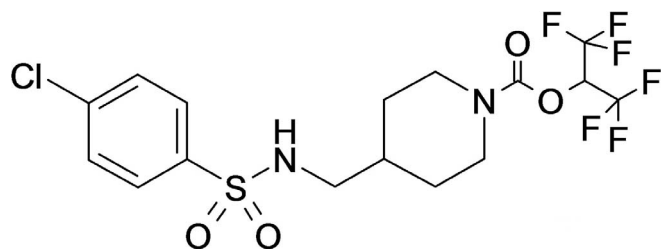


Figure 1 | Chemical structure of SAR127303.

methylcellulose and the addition of 0.1% Tween 80 (Sigma RBI) (unless otherwise indicated) in *in vivo* studies and suspended in DMSO at 10 mM in *in vitro* experiments. Formalin (Sigma RBI) was dissolved in 0.9% saline and phenylbenzoquinone (Sigma RBI) was solubilized in a 0.9% saline solution containing 1% alcohol. SSR411298 and JZL184 were synthesized by Sanofi Medicinal Chemistry. Doses refer to the weight of the free base. All drug solutions were prepared fresh daily.

In vitro selectivity profile. The effect of SAR127303 on approximately 240 different receptors, ion channels, enzymes, transporters, kinases and serine hydrolases (see Supplementary Material and Supplementary Table S1 for details) was evaluated at contract research organizations (CEREP, ActivX) using established protocols or through internal studies. IC₅₀ were determined in case significant activity was observed at 10 μM (≥50% inhibition).

Activity of SAR127303 in MAGL biochemical assay. Biochemical activity of SAR127303, reference MAGL inhibitor JZL 184 and FAAH inhibitor SSR411298 were assessed using human recombinant MAGL (rhMAGL) and 4-nitrophenylacetate as a substrate using MAGL Inhibitor Screening kit (Cayman Chemical, Cat. 705192) according to manufacturer’s instructions. IC₅₀ was calculated using GraphPad Prism version 4.00 for Windows (GraphPad Software, Inc.).

LC-MS evidence of covalent modification of MAGL Ser122 by SAR127303. Recombinant human MAGL (2.5 μM) was pre-incubated with different concentrations of SAR127303 for 2 hours. Resulting samples were digested with chymotrypsin overnight. The mixtures were then injected into AB Sciex Qtrap 5500 LC/MS/MS System for quantitative monitoring of two unmodified peptides containing Ser 122 (LHSMGGAIAIL is the peptide and LLHSMGGAIAIL is with a mis-cleavage). Peptide derived from MAGL C-terminus (HKELPEVTNSVF) was used as control. Separation was performed on 1.0 × 150 mm Waters HSS T3 LC column with the flow rate of 0.2 mL/min.

Protein crystallization and data collection. Crystals of the apo-protein were obtained in MES 50 mM pH 6.0, MPD 40% (v/v) at 4°C. They were used for soaking experiments in presence of 1 mM of SAR127303 overnight at 4°C. The cryo-protecting solution contained 10% MPD (v/v), 30% PEG2000 MME and 1 mM of SAR127303. A 2.36 Å resolution dataset was collected at ESRF (beamline ID14-2). The structure of MAGL-SAR127303 was solved by molecular replacement using the apo-structure (PDB code 3JW8) as the search model. Protein cloning, expression and purification were described elsewhere³⁹. Coordinates and structure factors for MAGL in complex with SAR127303 have been deposited in the Protein Data Bank under the accession code 4UUQ.

Plasma exposure and brain penetration. SAR127303 was administered p.o. to CB17 SCID male mice (Charles River) in 20% Glycofurol, 10% Vitamin E TPGS in water. Plasma and brain samples were harvested at the indicated time points and stabilized in the presence of 0.4 mg/ml PMSF. SAR127303 was detected in plasma and in tissue using established LC/MS protocols.

Functional activity. MAGL activity of brain homogenates prepared from mice treated with SAR127303. Mice were euthanized 1 hour after oral administration of SAR127303 or vehicle. Brains were rapidly removed and immediately frozen at –80°C for conservation. The day of MAGL activity measurement, brains were homogenized in buffer containing Tris-HCl 10 mM (pH=8.0); 150 mM NaCl; 1 mM EDTA. The hydrolysis reaction was performed at room temperature in phosphate buffer 50 mM, pH8, fatty acid free BSA 1 mg/ml, in 96 wells filtration plates. Briefly, mouse brain homogenates (treated by SAR127303 or vehicle) were incubated 20 minutes with 50 μM of a mix of cold and tritiated 2-oleoylglycerol radiolabeled on its glycerol moiety (0.027 μCi/well). The reaction was stopped by the addition of activated charcoal (activated charcoal 5 M diluted in NaCl 1.5 M and HCl 0.5 M). Plate was then mixed for 10 minutes. The [³H]glycerol produced was recovered by vacuum filtration prior to scintillation counting (plate reader). MAGL activity for each mouse is expressed in % of MAGL activity measured in vehicle treated mice. A non specific MAGL activity, obtained by the measure of 2-AG hydrolysis in the presence of an excess of SAR127303 in wells containing vehicles treated mice brain homogenate, is subtracted from each value. This non specific hydrolysis represents about 20% of total 2-AG hydrolysis. Data were analyzed with a one-way ANOVA followed, when appropriate, by a Dunnett’s test.

Brain lipid profiling. The levels of several monoacylglycerols (MAGs) and free fatty acids (FFAs) were measured in the whole brain of mice that received vehicle or SAR127303 (MAGs: 10 or 30 mg/kg, p.o.; FFAs: 10, 30 or 60 mg/kg p.o.) and that were sacrificed 4, 8 and 24 h later. Brain tissues were rapidly homogenized in Tris-EDTA buffer (pH=7.4) using Precellys 24 tissue homogenizer and an aliquot was used for protein measurements. Lipids were extracted using chloroform/methanol solvent (1:2) containing 0.025 N HCl. After centrifugation and supernatant withdrawal, the samples were dried by gentle nitrogen flow. The residue was reconstituted in methanol solvent for LC/MS analysis. Quantitation of monoacylglycerols (MAGs) was performed on the ABSciex QTrap 5500 MS system coupled with Agilent 1290 Infinity UHPLC system using Waters Xbridge C18 column (2.1 × 100 mm) for separation. MAG abundance was normalized to protein concentration in the sample. The following MAGs were measured: MAG 16:0,



1-hexadecanoyl-rac-glycerol; MAG 18:0, 1-monoacylglyceride; MAG 18:1, 1.1-(11Z-Octadecenoyl)-rac-glycerol; MAG 18:2, 1-(9Z,12Z-octadecadienoyl)-rac-glycerol; MAG 20:4, 2-arachidonylglycerol. The following FFAs were measured: Palmitic acid, palmitoleic acid, stearic acid, vaccenic acid, linoleic acid, arachidonic acid and docosahexaenoic acid. Two-way ANOVA (treatment x time) was used to assess overall effect of treatment, and Dunnett's post test was used to compare differences between treatment groups.

Levels of 2-AG, AEA, PEA and OEA in the hippocampus of mice treated with SAR127303. The levels of 2-AG, AEA, palmitoylethanolamide (PEA) and oleoylethanolamide (OEA) were measured in the hippocampus of CD1 mice that received either vehicle (0.1 mL/10 g, p.o.) or SAR127303 (8 mg/kg, p.o.) and that were sacrificed 1, 2, 6 and 24 h later. Hippocampus (right and left) were frozen and weighed before storage until analysis. For 2-AG analysis, each sample was homogenized in 1 mL of heptane/isopropanol 3/2 containing 1 μ M of 2-AG-d8 (Internal standard for 2-AG), centrifuged at 12000 g for 7 minutes at 4°C.

Supernatant was evaporated and dissolved in 150 μ L of acetonitrile (ACN) and 150 μ L of H₂O for injection (100 μ L) in an on-line SPE-LC-MS/MS. The on-line SPE (Solid Phase Extraction) coupled to the LC (Liquid Chromatography) was performed with a "Symbiosis" apparatus from SparkHolland using a C18 HD, 7 μ M cartridge (2 \times 10 mm as internal diameter \times length) and a Hypersil gold C18 (1.9 μ m, 50 \times 2.1 mm) column respectively for the on-line extraction and separation. The elution was performed at 0.25 mL/min with a ACN/H₂O + ACNH₄ 2 mM gradient, both solvent containing 0.1% of HCOOH. The end eCBs were identified and quantified by a triple quadrupole mass spectrometry detector (Quantum Ultra from Thermo Electron Corporation) equipped with an ESI probe and working in the SRM mode (Selective Reaction Monitoring). The concentrations of each compound were calculated according to external calibration method. Data were analyzed with a one-way ANOVA followed by a Dunnett's test.

Mouse tetrad experiments and elevated plus-maze. The potential cannabimimetic activity of SAR127303 in 8-week-old OF1 mice (Charles Rivers Laboratories, L'Arbresle, France) was evaluated using the following indices: locomotor activity, nociception in the tail flick test, catalepsy in the bar test, and hypothermia. The effects were compared to those obtained with the CB1 receptor agonist, WIN55,212-2 at 15 mg/kg. In addition, SAR127303 effects on anxiety-related behaviors were assessed in the elevated plus-maze test. For determining hypomotility each mouse was placed in an actimeter device consisting of a cylinder (20 cm diameter, 9.5 cm high, Apex, France) equipped with two perpendicular light beams located 1.5 cm above the floor and locomotor activity (number of interrupted light beams) was recorded for a period of 30 min. The tail flick analgesia meter consists of a stimulation unit (containing the halogen lamp for the heat stimulus) and an electronic control unit (Columbus Instruments, Columbus, Ohio, USA). The mouse is placed with its tail protruding within a restraining tube on the platform of the Stimulus Unit. The animal's tail is positioned on a slot of adjustable width equipped with a groove that guarantees a correct placement of the rodent's tail. A remote foot-switch controls the test start/stop allowing rapid hands-free experiments. A photo beam detects the tail flick and the latency is automatically presented on a digital display on the Control Unit. Measurements of reaction time are given with a 0.01 s precision. A cut-off time of 20 s is set to avoid tissue damage. Catalepsy was evaluated using the bar test, in which the front paws of each subject were placed on a rod (0.75 cm diameter) that was elevated 4.5 cm above the surface. Mice that remained motionless with their paws on the bar for 10 s (with the exception of respiratory movements) were scored as cataleptic. Hypothermia by inserting a thermocouple probe 2.0 cm into the rectum. The elevated plus-maze test is based on that described by Lister et al (1990). The testing apparatus was made of grey polyvinylchloride (PVC) and elevated to a height of 48 cm with two open/unprotected (30 \times 5 cm) and two enclosed arms (30 \times 5 \times 20 cm) arranged so that the arms of the same type were opposite to each other. To prevent mice falling off, a rim of Plexiglas (0.25 cm high) surrounded the perimeter of the open arms. The light intensities measured in the open arms, closed arms and on the central platform were 70, 20 and 50 lux, respectively. For testing, mice were placed in the center of the maze facing a closed arm, for a free exploration period of 5 min. A camera was mounted above the maze and a video tracking software (EthoVision XT 3.0, Noldus, Wageningen, Netherlands) was used to record the behavior of mice. Results are expressed as mean ratio of time spent in open arms to total time spent in both open and closed arms. SAR127303 and the positive control, diazepam, were administered p.o. 60 min before testing. Data were analyzed with a one-way ANOVA followed, when appropriate, by a Dunnett's test.

Effects of SAR127303 in models of pain. The phenylbenzoquinone (PBQ)-induced writhing model of acute visceral pain in mice. PBQ (2 mg/kg in 10 mL/kg) or vehicle was injected i.p. in male OF1 mice (24–29 g, Charles Rivers Laboratories, L'Arbresle, France). Each mouse was placed in an individual box containing sawdust and the intensity of nociceptive behavior was quantified by counting the total number of writhes (contraction of the abdominal muscle together with a stretching of hind limbs or rotation of the trunk) occurring between 5 and 15 min after the PBQ injection. The intensity of the writhing response was expressed as the total writhing over the 10 min period. Experiment 1 (dose-response): SAR127303 was administered orally 60 min prior to testing; Experiment 2 (antagonism by the CB1 receptor antagonist, rimonabant): SAR127303 and rimonabant were administered orally or intraperitoneally 60 and 30 min prior to testing, respectively. Experiment 3 (antagonism by the CB2 receptor antagonist, SR144528): SAR127303 and SR144528

were administered orally or intraperitoneally 60 or 90 min prior to testing, respectively. Data were analyzed with a Kruskal-Wallis test followed, when appropriate, by a Wilcoxon two-tailed comparisons test. These analyses, and all subsequent ones were performed using the SAS software (SAS Institute Inc., Cary, NC, USA).

The formalin test of inflammatory pain in mice. Twenty microliters of diluted formalin (2.5%) were injected subcutaneously (s.c.) into the dorsal surface of the right hind paw of male OF1 mice (26–30 g, Charles Rivers Laboratories, L'Arbresle, France) using a microsyringe. The incidence of spontaneous behavior was scored every 3 minutes for a period of 45 minutes after formalin injection. Briefly, the scores were: 0 = normal behavior of the hind limb to support the body; 1 = slight touching of the injected paw on the glass surface to lightly support or not support the body; 2 = total withdrawal of the injected paw; and 3 = licking, biting or shaking of the injected paw.

The data collected between 0 and 15 minutes post-formalin injection represent the acute phase (nociceptive phase), and the data collected between 15 and 45 minutes represent the late phase (inflammatory phase). Experiment 1 (acute dosing): Sixty minutes before the formalin insult, the animals were orally administered with the vehicle or SAR127303; Experiment 2 (repeated dosing): SAR127303 was administered once-a-day for five consecutive days. The last dosing occurred on day five 60 min before formalin injection. The areas under the curves (AUCs [0–15 min] and [15–45 min]) of the vehicle-treated and SAR127303-treated group at 10 mg/kg (acute and repeated dosing) were compared with a Wilcoxon test. We have tested the unique dose of 10 mg/kg in this test because it produces a nearly complete inhibition of both MAGL activity and writhes in the PBQ test. This latter being a good predictor of dose-efficacy in the formalin test.

Effects of SAR127303 in models of cognitive processes. In vitro long term potentiation (LTP). Following halothane anaesthesia, the brain of 3- to 8-week-old rats (Janvier Labs, Le Genest Saint Isle, France) was dissected and hippocampal slices were prepared using a cooled vibroslicer (Leica Biosystems, Nanterre, France). Following recovery for at least 1 hour at room temperature in oxygenated artificial cerebrospinal fluid (aCSF containing in mM: NaCl 126; KCl 3.5; NaH₂PO₄ 1.1; CaCl₂ 2.2; MgCl₂ 1.3; NaHCO₃ 25; D-glucose 10; pH 7.2–7.4), slices were transferred on microelectrode arrays (MEAs, Multi Channel Systems, Reutlingen, Germany) under visual control using a CCD camera (Microvision Instruments, Evry, France). The hippocampal slices were placed in close contact with the largest number of recording electrodes within the CA1 area. The field population spikes (fPS) were elicited in the hippocampal CA1 area every 30 s by injection of biphasic currents (–120 μ A/ +120 μ A, 60 μ s, MC Stimulus, Multi Channel Systems). fPS amplitudes were recorded 10 minutes before and 30 minutes after LTP induction (High Frequency Stimulation, 100 Hz for 1 second, twice with a 30 seconds interval) in the absence (control) or in the presence of SAR127303. SAR127303 was superfused at 1 or 10 μ M in a CSF, 30 minutes before and 30 minutes after LTP induction. All recordings were performed at a controlled temperature of 32°C (\pm 1°C).

Effects of 2-AG and SAR127303 on [³H]ACh release evoked by electrical depolarisation in rat hippocampal slices. Tissues were obtained from male Sprague-Dawley rats (200–250 g). After death, brains were removed and hippocampus was quickly dissected out. Hippocampal slices (500 μ m) were suspended in 20 mL Krebs buffer saturated with 5% CO₂ in O₂. Composition of Krebs medium (in mM) was: NaCl 125, KCl 5, CaCl₂ 1.2, MgCl₂ 1.1, NaHCO₃ 20, NaH₂PO₄ 1.2, glucose 10, pH 7.4. [³H]-Acetylcholine ([³H]-ACh), 100 nM was added and the incubation was carried out at 37°C for 30 min. After incubation, slices were rinsed three times with Krebs medium. 30 μ L of Krebs medium containing hippocampal slices were transferred into each superfusion chamber between two platinum electrodes, 1 cm apart (Brandel system, USA). The slices were superfused at a rate of 0.5 ml/min. Collection of 3 min serial fractions (1.5 mL) began after a 42 min wash period. Electrical stimulation consisted of 2 ms monophasic rectangular pulses (2 Hz, 160 mA, 1 min) (Brandel stimulator, USA) and was done during the 6th fraction. CTP was perfused from 9 min before the electrical stimulation to the end. At the end of the experiments, tissue slices were collected and solubilized in Soluene-350 (Perkin-Elmer). Total tritium activity in the 3 min fractions and samples with solubilized tissue slices was measured by liquid scintillation spectrometry. The fractional efflux of [³H]-ACh was estimated as a percentage of the amount of radioactivity in the superfusate fraction relative to the total amount of radioactivity in the slices at the beginning of the experiment. The amount of radioactivity at the beginning of the experiment was estimated as the sum of radioactivity measured in the solubilized slices at the end of the super-fusion and the total radioactivity collected in the medium samples from the beginning to the end of the experiment. To determine stimulated release, the basal efflux of radioactivity in the fraction prior to stimulation was subtracted from each of the subsequent five electrical depolarization fractions, the values then being summed. The statistical analyses of the biochemical results were performed using Student's t-test.

Effect of SAR127303 on in vivo hippocampal ACh release in rats.

Surgery and microdialysis. Sprague-Dawley rats (Charles River, France) weighing 250–350 g, were anaesthetized with Zoletil® 50 (60 mg/kg, i.p.) in NaCl (0.9%, 10 mL/kg of body weight) and placed in a stereotaxic apparatus. A guide cannulae was implanted at the following coordinates according to the atlas of Paxinos and Watson³⁰: 5.3 mm posterior to bregma, 4.8 mm lateral to bregma and 8 mm down from the dorsal surface). The microdialysis probe (4 mm outer diameter 0.5 mm; CMA 12, CMA/Microdialysis, Stockholm, Sweden) was perfused at a constant flow



rate of 2 $\mu\text{L}/\text{min}$ using a microinjection pump (CMA 100, CMA/Microdialysis, Stockholm, Sweden) with a gassed Ringer's solution containing (in mM): NaCl, 147; KCl, 4; CaCl_2 , 1.2; MgCl_2 , 1; pH 7.4. To reduce ACh degradation in the dialysate, 0.3 μM of neostigmine (Sigma-Aldrich, Saint Quentin Fallavier, France) was added to the Ringer's solution perfused in the probe. Microdialysis sampling started 90 min after the probe was placed into the hippocampus. Serial samples were collected at 20 minutes and analyzed using high performance chromatography (HPLC) with electrochemical detection. The position of the probe was verified histologically at the end of extracellular ACh experiment⁴¹.

Treatment. SAR127303 was suspended with Tween 80 (Polyoxyethylene sorbitan mono, 1 drop, Sigma-Aldrich) and methylcellulose 0.6% (Sigma-Aldrich, Saint Quentin Fallavier, France) in distilled water and was administered intraperitoneally (i.p.) (5 mL/kg body weight) after a control period of 60 minutes.

Determination of extracellular ACh. ACh levels were measured in 20-min dialysate samples (40 μL) by an high pressure liquid chromatography system (HPLC) and electrochemical detection using a similar technique previously described by Damsma et al.⁴². Briefly, 40 μL of samples were injected through a refrigerated Microsampler (CMA-200; Carnegie Medicine AB, Stockholm, Sweden) onto a reverse-phase C18 column (Kromasil 5 μm , 50 \times 2 mm) preloaded with sodium laurylsulphate (Sigma-Aldrich, Saint Quentin Fallavier, France). The mobile phase consists of a 0.15 M potassium phosphate buffer (pH = 8.0) containing 600 mg/L of tetramethylammonium chloride (Merck, Nogent sur Marne, France) and was delivered by a dual-piston HPLC pump Waters 515 (Waters Associates, CA, USA) at a flow rate of 0.5 mL/min. ACh was converted into hydrogen peroxide and betaine in a post-column enzyme-reactor (BAS.MF-6151). Hydrogen peroxide resulting from the enzymatic reaction was then detected using a platinum electrode (Antec, Leiden, The Netherlands) set at + 500 mV versus an Ag/AgCl reference electrode. The chromatographic column, the enzyme reactor and the electrochemical cell were maintained at 30°C. The detection limit of the assay was approximately 3 pg/40 μL . Extracellular ACh levels (pg/40 μL) were expressed by comparing the area of the ACh peak measured in the dialysate with that detected in a standard solution. The area corresponds to the oxidation current of ACh and is proportional to the concentration of the neurotransmitter in the dialysate sample.

Statistical analysis and data presentation. ACh levels in samples were converted to a percentage of the mean value of the 3 fractions before treatment (fractions -40, -20 and 0 minutes). The effect of SAR127303 in brain regions was presented by comparing to baseline variation during the post-treatment period (fractions 20 to 140 minutes). The stability of the 3 fractions used to define the 100% basal period was checked by performing a two-way ANOVA with repeated measures on basal ACh levels according to "Treatment" and "Time" (repeated factor) at -40, -20 and 0 minutes. For the effect of SAR127303, a two-way ANOVA with repeated measures was carried out on transformed percent ACh levels from 20 to 140 minutes according to "Treatment" and "Time" (repeated factor). In case of significance of the "Treatment" and "Time" interaction, a Winer analysis is performed to study the global effect of factor "Treatment" for each level of "Time" factor. Then, if the "Treatment" global effect is significant at a given level of "Time", a Dunnett's test is performed to compare the treatment versus vehicle treated group at this (these) time(s).

The novel object recognition task in mice. The test apparatus was based on that described by Ennaceur and Delacour⁴³ in rats and adapted for use in mice⁴⁴. The apparatus consisted of a uniformly lit (20 lx) PVC enclosure (52 L \times 52 W \times 40 H cm) with a video camera positioned 160 cm above the bench. The observer was located in an adjacent room fitted with a video monitoring system. The experiment consisted of 3 sessions. During a first session, male Swiss mice (25–30 g; Janvier Labs, Le Genest Saint Isle, France) were allowed to become familiar with the experimental environment for 5 min (S1). Time spent active (animal moving around with or without sniffing and exploration) was measured. 24 hours later, the animals were again placed in the enclosure in the presence of two identical objects for the amount of time necessary to spend 15 s exploring these two objects to a limit of 5 min (exploration was defined as the animal having its head within 2 cm of the object while looking at, sniffing, or touching it) (S2). After a forgetting interval of 60 min, mice were placed again in the enclosure with a previously presented familiar object and a novel object for a period of 4 min (S3). Time spent exploring the familiar and novel objects was recorded. For a short-term forgetting delay, during the recall session, normal mice spent more time exploring the novel object compared to the familiar one. That reflects a remembering of the familiar object. Short-term memory was impaired by MK-801 injection, mice spending the same amount of time exploring both object, reflecting a forgetting of the familiar object and a short-term visual memory deficit. Experiment 1 (dose-response): SAR127303 was administered orally immediately following S2. Experiment 2 (repeated): SAR127303 was administered orally twice-a-day for 4 days. The last administration was performed on day 5, immediately after S2. Experiment 2 (antagonism by rimonabant): SAR127303 and rimonabant were administered orally or i.p., respectively, immediately following S2. Data were expressed as ratio of novelty index: [(time exploring novel object)/(time exploring novel object + time exploring familiar object) \times 100]. Data (time exploring each of the 2 objects, in seconds) were analyzed for habituation and acquisition sessions, using a one-way ANOVA assessed on the variables "locomotion" and

"time" necessary to reach 20-second active exploration for 2 identical objects, respectively. For the recall test sessions, the novelty index ratio (expressed in percentage) was analyzed with a one-way ANOVA followed, when appropriate, by a Dunnett's (Experiments 1) or Newman-Keuls (Experiments 2 and 3) analysis for individual comparisons. These analyzes, and all subsequent ones were performed using the SAS software (SAS Institute Inc., Cary, NC, USA).

The Y-maze test in mice. The Y-maze consisted of 3 arms in gray PVC in the shape of a Y. Arms were 28 cm long, 6 cm wide with walls 15 cm high. Movement was tracked manually using homemade software by an experimenter located in an adjacent room via a camera mounted directly above the maze. The animal was placed in an arm facing the center (Arm A) for 5 min. A correct alternation occurred when the animal moved to the other 2 arms without retracing its steps (i.e. Arm A to B to C). Movements such as ABA were incorrect. Based on the movement over the entire session, the percentage of correct alternations was calculated (i.e. Total number of alternation \times 100)/(Total number of arm entries-2). SAR127303 was administered orally 60 min and PCP was given i.p. 30 min prior to testing. Thirty minutes later, NMRI mice (16–18 g, Janvier Labs, Le Genest Saint Isle, France) were placed in the apparatus and recording was started. Statistics performed on total arm entries and percentage alternation consisted of using a one-way ANOVA, followed by a post-hoc Dunnett's test for individual comparisons.

The Morris water maze in rats. The Morris water maze apparatus consisted of a PVC pool (1.20 m diameter \times 0.60 m high), filled with thermostated water (23 \pm 2°C) to a depth of 35 cm, with the addition of milk to render the water opalescent. A Plexiglas escape platform (12 cm diameter) was placed into the pool, 1 cm below the water surface and 10 cm from the wall. The test room contained several permanent extra-maze cues such as posters, flag, etc. on walls. A video-tracking camera (placed 200 cm above the center of the pool surface) monitored the trajectory of the rat [male Wistar Han strain, 225–250 g (Janvier Labs, Le Genest Saint Isle, France) at the start of the study] and the video signal was transmitted to a computer in an adjacent room and analyzed using the VIDEOTRACK® system (View Point Ltd, Champagne au Mont d'Or, France). The platform was placed at one of four possible cardinal locations NW, SE, NE, and SW, and NW for learning session 1, 2, 3, 4, and 5, respectively. Each learning session consisted of three trials, with a maximal duration of 120 s and an intertrial interval of 30 s. Latency times (in seconds) to find the hidden platform were recorded during each trial of each learning session. If the rat located the platform within the maximum time allowed (120 s), it was left on the platform for 30 s. If the rat did not locate the platform within the time limit, it was gently placed on it for a 30-s period. At the start of each trial of each day, the rat was gently placed at the periphery of the maze, opposite of the platform (ie for the first trial E, for the NW quadrant). For each subsequent learning session, a similar cardinal rule was applied (i.e. N, W, N, and E for the SE, NE and SW, and NW quadrant, respectively). All rats received administrations of SAR127303 (p.o.) or vehicle, 60 min before the first trial of each day. Data (latency times to reach the platform for each individual trial during the 3-day learning sessions were analyzed with a two-way ANOVA, with the treatment as the between factor, and the trials for each learning session as the within factor. Post-hoc analysis was performed with Newman-Keuls post-hoc tests. The data on the first trial were compared using an ANOVA to ensure that the groups do not display different performance levels at start.

Effects of SAR127303 in models of seizures. *The 6-Hz electroshock-induced seizures in mice.* SAR127303 (30 mg/kg) and the reference anticonvulsant agent levetiracetam (20 mg/kg) were administered orally or i.p. to OF1 mice (12–14 g) 60 or 30 min prior to test, respectively. An electrical stimulus (6 Hz, 0.2 ms rectangular pulse, 3 s duration, 32 mA) was applied to both corneas. Animals were closely observed and rated for seizure behavior according to a modified Racine scale⁴⁵. Kruskal-Wallis multiple comparisons test was used to assess potential differences between treatment groups.

The pentylenetetrazol (PTZ) seizure threshold test in mice. The seizure threshold was determined by the infusion of 8 mg/mL of PTZ at a rate of 0.7 mL/min via a flexible plastic catheter into the tail vein of freely moving OF1 mice (22–24 g) using an infusion pump. The convulsant dose for each endpoint was calculated in mg/kg PTZ. SAR127303 (30 mg/kg) and the reference benzodiazepine diazepam (3 mg/kg) were administered orally or i.p., 60 or 30 min prior to the beginning of PTZ infusion, respectively. One-way ANOVA was used to assess overall effect of treatment, and Dunnett's post test was used to compare differences between treatment groups.

The corneal kindling model in mice. C57BL/6J mice (22–24 g) received twice-daily subconvulsive corneal stimulations of 8 mA/0.8 ms at 60 Hz for 2 s for 11 days. Following the acquisition of kindling at day 5, mice were allowed a two-day stimulation free period. Stimulations were at least 90 min apart. Mice were considered kindled when displaying five consecutive stage five seizures according to a modified Racine scale. Mice were divided into the following groups: (1) Control: they were treated with saline from day 1 to day 5, and from day 8 to day 11; (2) Acute SAR127303: mice were treated with saline from day 1 to day 5, and from day 8 to day 10, and on day 11 they received a single oral administration of 30 mg/kg SAR127303; (3) Repeated SAR127303: these mice were administered 10 or 30 mg/kg SAR127303 orally once-a-day from day 1 to day 5, and from day 8 to day 10. On treatment days, animals were administered saline or SAR127303 after the second stimulation, except on day 11, where the administrations were performed between the two stimulations. Two-way ANOVA (treatment \times time) with repeated measures on



factor time was used to assess overall effect of treatment, and Winer post test was used to compare differences between treatment groups.

The kainic acid-induced seizures test in mice. SAR127303 (30 mg/kg) was administered orally to C57BL/6 mice (22–24 g) 30 min prior to the i.p. injection of 30 mg/kg kainic acid. Thirty min later, animals were closely observed and rated for seizure behavior according to a modified Racine scale⁴⁵. Kruskal-Wallis multiple comparisons test was used to assess potential differences between treatment groups.

Results

In vitro selectivity profile. SAR127303 behaves as a highly selective inhibitor of mouse and human MAGL ($IC_{50} = 3.8$ and 29 nM, respectively). With the exception of ABHD6, the drug does not modify the activities of other human serine hydrolases (e.g. FAAH, DPP7, APEH) (Figure S1) nor interact with a variety of potential targets, including 170 kinases, ion channels, neurotransmitter transporters, and receptors, including CB1 and CB2.

Activity of SAR127303 in MAGL biochemical assay. SAR127303 potently inhibited rhMAGL ($IC_{50} = 48$ nM). Published MAGL tool compound JZL184 has lower potency ($IC_{50} = 0.48$ μ M), while FAAH inhibitor SSR411298 did not show any activity in this assay ($IC_{50} > 10$ μ M) (Figure 2).

LC-MS evidence of covalent modification of MAGL Ser122 by SAR127303. Mass spectrometry based mapping identified Ser 122 as the covalent binding site for SAR127303 (data not shown). Subsequent treatment of recombinant human MAGL with different concentrations of SAR127303 resulted in dose-dependent modification of MAGL protein, as indicated by the decrease in unmodified MAGL peptides containing Ser 122. The abundance of the control peptide derived from MAGL C-terminus was not affected (Figure 3).

Protein crystal structure. MAGL inhibitor JZL184 has a chemical structure which is close to that of SAR629 described elsewhere³⁹. They both adopt a Y-shaped structure and their binding modes to human MAGL are similar and were described either by X-ray crystallography³⁹ or molecular modelling³⁰. The chemical structure of SAR127303, described here, does not possess a Y-shape and its binding mode, revealed by X-ray crystallography, shows that it can adopt two slightly different conformations. Indeed, as for the MAGL-SAR629 structure, the complex MAGL-SAR127303 crystallizes with two molecules in the asymmetric unit. Both molecules, although globally similar, adopt some structural differences as depicted in figure 4A. These differences mainly concern the position of the α -helix A4 of the LID and its surrounding loops.

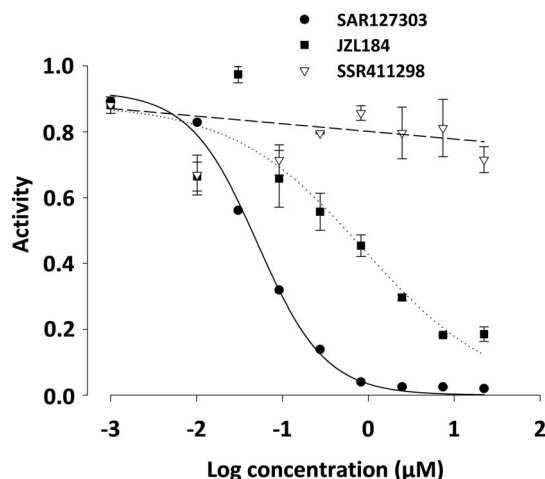


Figure 2 | Activity of SAR127303 in MAGL biochemical assay. Data are presented as mean \pm S.D.; $N=3$. SAR127303 and JZL184 are MAGL inhibitors; SSR411298 is a FAAH inhibitor.

A.

MPEESSRRTTQSPYQDLPHLVNADGQYLFCRYWKPTGTPKALIFV
SHGAGEHSGRYEELARMLMGLDLLVFAHDHVGHGQSEGERMVVS
DFHVFVRDVLQHVDSMQKDYPGLPVFLLGHSMMGGAIILTAAERP
GHFAGMVLISPLVLANPESATTFKVLAAKVLNVLNLSLGPIDSSVLS
RNKTEVDIYNSDPLICRAGLKVCFGIQLLNAVSRVERALPKLTPVFLLL
QGSADRLLCDSKGAYLLMELAKSQDKTLKIYEGAYHVLHKELPEVTNS
VFHEINMWVSQRTATAGTASPP

B.

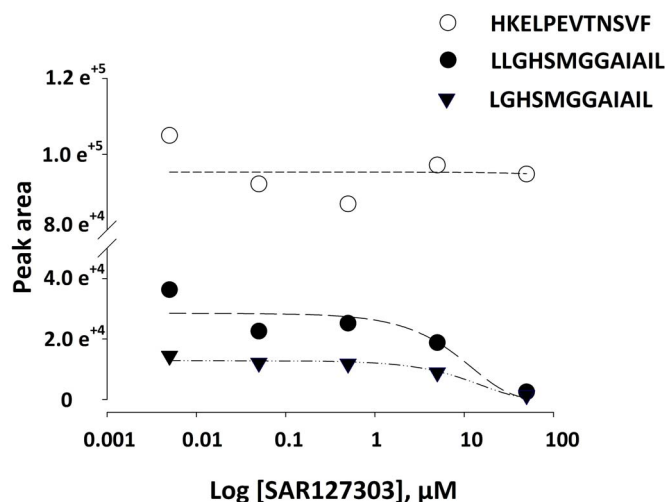


Figure 3 | LC-MS evidence of covalent modification of MAGL Ser122 by SAR127303. (A) MAGL protein sequence. Peptide containing Ser122 and control peptide sequences are underlined. (B) Dose-dependent decrease in unmodified Ser122-containing peptides in the presence of SAR127303.

One of these loops leads to different interactions with SAR127303 in molecule A and B in the crystal.

SAR127303, in return also depicts a slightly different orientation of its sulfonyl moiety. This leads to some differences in the protein-ligand interactions between molecule A and B (Figure 4B).

Aside from the covalent bond with Ser132, SAR127303 interacts with MAGL in the following way: the carbonyl oxygen of the carbamate function is H-bonded to main-chain nitrogen atoms of Ala61 and Met133, the hexafluoro-propanol moiety being removed during catalysis. The protein interaction with the piperidine moiety occurred through van der Waals interactions on one side with Leu251 but makes no contact on the other side. One oxygen atom of the sulfonyl function interacts in both molecules of the asymmetric unit with Asn162 main-chain nitrogen. In molecule A, this sulfonyl oxygen further makes water-mediated interactions with Asn162 side-chain nitrogen and Leu251 main-chain carbonyl oxygen. In molecule B, a water molecule is found H-bonded to the nitrogen atom of the main scaffold, but seems too distant to any other atom of the protein. The chloro-phenyl moiety of SAR127303 fits in a pocket lined by Leu215, Gly220, Leu223 and Leu224 residues in one side and Ser165, Ala166 in the other side. Gly220 main-chain and, only in molecule A, Ser165 side-chain oxygen atoms are the only polar atoms at a short distance of the chloro-phenyl moiety. The two different binding modes observed here can be explained by the fact that the loop to which belongs Asn162 is very flexible and the residues interacting with the chloro-phenyl moiety of SAR127303 (Ser165, Ala166) are not localized equivalently in both molecules of the asymmetric unit, resulting in different binding modes for the inhibitor.

It is important to note that several constructs have been tested to maximize success in expression rate and subsequent purification and crystallization. The best construct in terms of crystallizability and

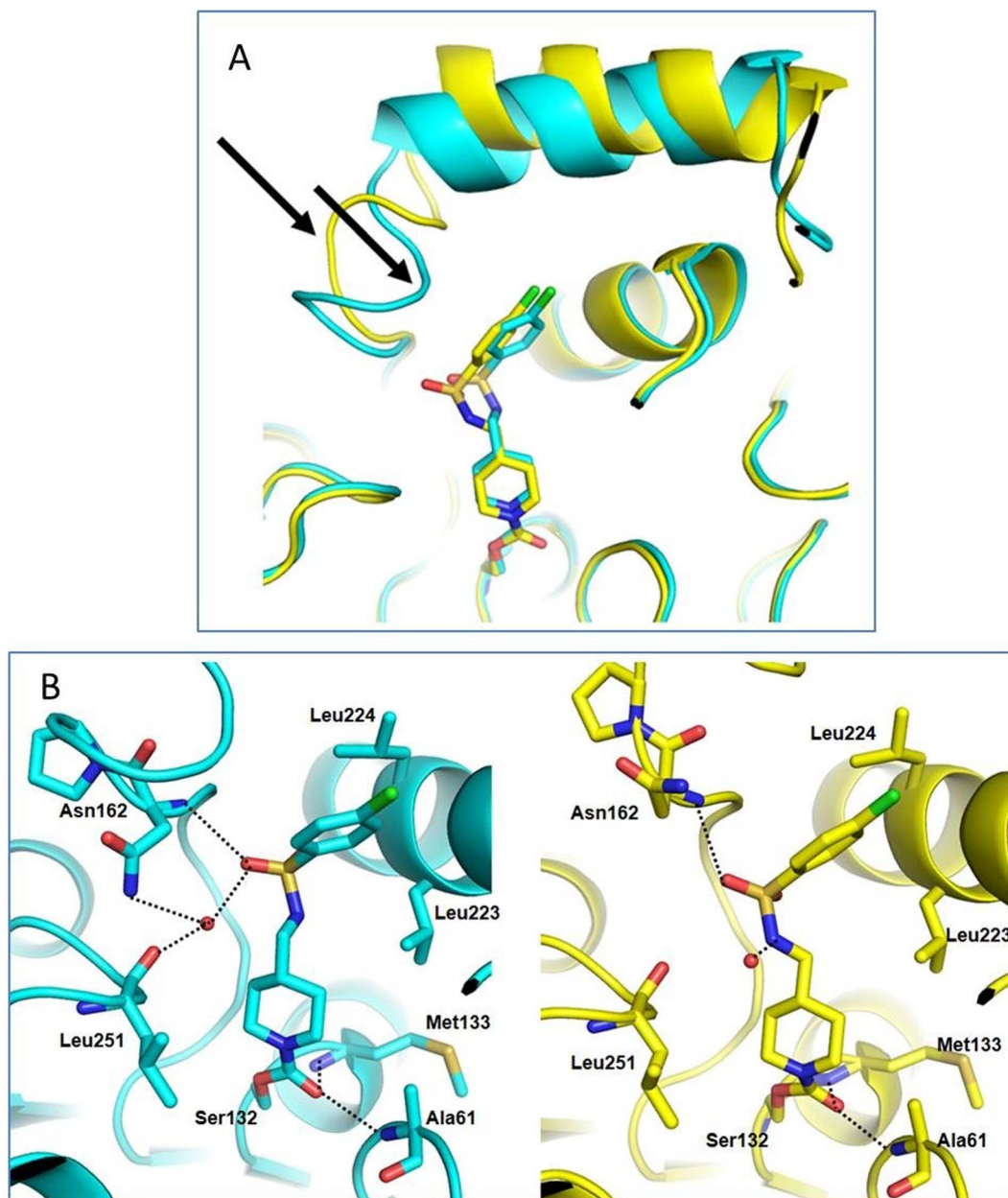


Figure 4 | A. Superimposition of SAR127303 active site in both molecules of the asymmetric unit (molecule A in cyan, molecule B in yellow). The flexible loops, interacting with the chlorophenyl and sulfonyl moieties of SAR127303 are pointed by arrows. B. MAGL-SAR127303 interactions in molecule A (cyan) and B (yellow). Hydrogen bonds are depicted as black dashes.

expression was His-1-1313. The purified isoform of human MAGL (Q6IBG9_HUMAN) has 313 aminoacids in comparison to 303 for the isoform described previously (Q99685_HUMAN), which explains the numbering difference (Ser122 in the LC-MS experiment vs Ser132 here).

Brain penetration and exposure. Single oral administration of SAR127303 at 10 and 30 mg/kg resulted in near dose-proportional increase in compound concentration in mouse plasma and brain. Plasma and brain C_{max} were observed at 4 hours after SAR127303 administration (Figure S2 and Table S2).

Functional activity. MAGL activity of brain homogenates prepared from mice treated with SAR127303. SAR127303 decreased MAGL activity in mouse brain in a dose-dependent fashion, an effect which reached statistical significance at 3 mg/kg p.o. [$F(5,36) = 42.09, P < 0.001$] (Figure 5A). Time-course analysis indicated that

enzyme activity was inhibited markedly for up to 6 hours after administration at the doses tested. Although at 24 hours post-administration, enzyme activity tended to return to baseline levels, it remained significantly inhibited [$F(4,30) = 188.26, P < 0.001$] (Figure 5B).

Brain lipid profiling. Treatment with SAR127303 (10 and 30 mg/kg p.o.) resulted in significant increase in major MAGL substrate in the brain, 2-arachidonoylglycerol [2-AG, MAG20:4: $F(4,27) = 2.70, P < 0.05$]. Basal concentrations of 2-AG at 4, 8 and 24 hours were 248, 218 and 209 $\mu\text{g/ml}$, respectively. Levels of other monoacylglycerols were not significantly altered, highlighting exquisite specificity of SAR127303 [MAG16:0: $F(4,27) = 0.19, P = 0.94$; MAG18:0: $F(4,27) = 1.95, P = 0.13$; MAG18:1: $F(4,27) = 0.43, P = 0.78$; MAG18:2: $F(4,27) = 0.68, P = 0.61$]. In the 10 mg/kg group, 2-AG levels declined to basal levels by 24 hours. In contrast, it remained elevated in 30 mg/kg-treated mice 24 hours after compound admin-

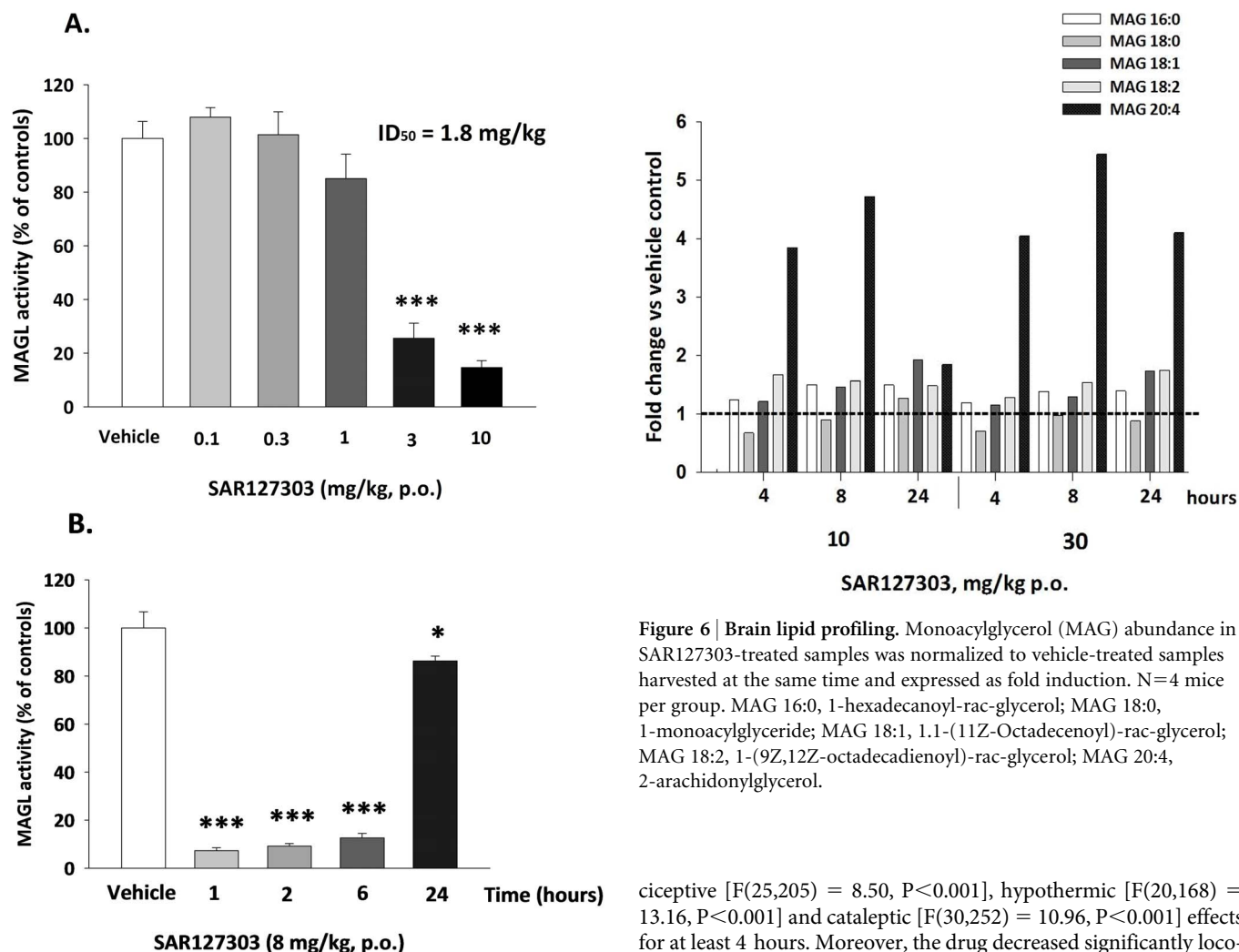


Figure 5 | MAGL activity of brain homogenates from mice treated with SAR127303. Data are presented as mean + S.E.M.; * $P < 0.05$, *** $P < 0.001$; $N = 7$ per group.

istration (data not shown). Figure 6 shows that at 10 mg/kg, SAR127303, produced a 4-fold increase in 2-AG as compared to control levels. This effects lasted at least for 8 hours. The highest dose of SAR127303 (i.e. 30 mg/kg) produced a 4- (at 4 and 24 hours) or 5- (at 8 hours) fold increase in 2-AG. None of the FFAs measured were modified significantly by SAR127303 up to 60 mg/kg p.o. (data not shown).

Levels of 2-AG, AEA, OEA and PEA in the hippocampus of mice treated with SAR127303. SAR127303 significantly increased hippocampal 2-AG levels at 8 mg/kg p.o. [$F(4,43) = 229.22$, $P < 0.001$], but failed to affect AEA, PEA and OEA levels in this structure when administered at 8 mg/kg p.o. (Figure 7). The effect on 2-AG reached statistical significance at 1, 2 and 6 h post-administration (Dunnett's test for all time-points: $P < 0.001$). Twenty-four hours after the administration of the drug, 2-AG levels returned to baseline ($P = 0.94$) (Figure 7).

Mouse tetrad experiments and elevated plus-maze. SAR127303 did not elicit antinociception in the tail-flick test, catalepsy, hypothermia, nor decrease locomotor activity at doses up to 30 mg/kg p.o. over the entire 24-h testing period (Figure S3). Moreover, free observation revealed no hyperreflexia as observed with previous MAGL inhibitors. This was in contrast to the CB1 receptor agonist WIN55,512-2 at 15 mg/kg i.p., which produced significant antino-

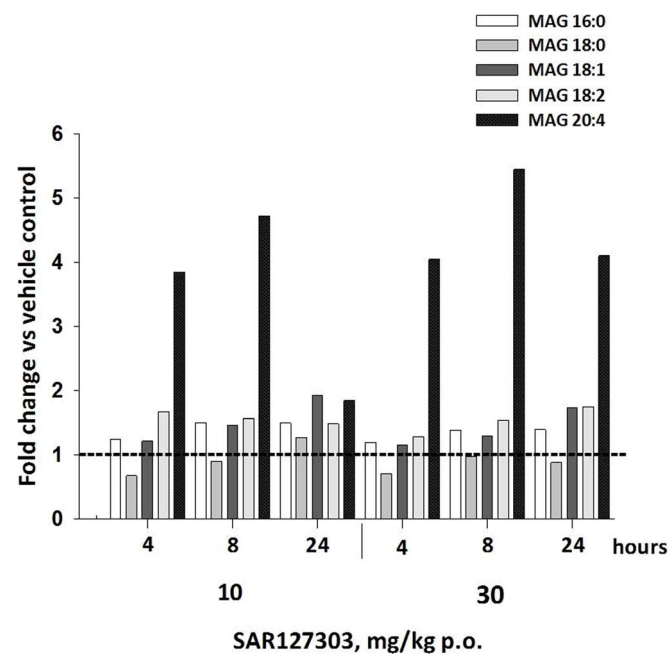


Figure 6 | Brain lipid profiling. Monoacylglycerol (MAG) abundance in SAR127303-treated samples was normalized to vehicle-treated samples harvested at the same time and expressed as fold induction. $N = 4$ mice per group. MAG 16:0, 1-hexadecanoyl-rac-glycerol; MAG 18:0, 1-monoacylglyceride; MAG 18:1, 1,1-(11Z-Octadecenoyl)-rac-glycerol; MAG 18:2, 1-(9Z,12Z-octadecadienoyl)-rac-glycerol; MAG 20:4, 2-arachidonylglycerol.

ciceptive [$F(25,205) = 8.50$, $P < 0.001$], hypothermic [$F(20,168) = 13.16$, $P < 0.001$] and cataleptic [$F(30,252) = 10.96$, $P < 0.001$] effects for at least 4 hours. Moreover, the drug decreased significantly locomotor activity [$F(5,60) = 12.28$, $P < 0.001$]. In the elevated plus-maze, SAR127303 at 10 mg/kg p.o. significantly decreased percentage of time in open arms, while the prototypical anxiolytic drug diazepam produced the opposite effects [$F(4,55) = 9.93$, $P < 0.001$] (Figure S4).

Effects of SAR127303 in models of pain. *The phenylbenzoquinone (PBQ)-induced writhing model of acute visceral pain-like behavior in mice.* In the dose-response experiment, Kruskal-Wallis analysis indicated a global main effect of treatment ($\chi^2 = 25.418$, $P < 0.001$). Further analysis showed that SAR127303 produced a significant reduction in writhing response at 1 and 3 mg/kg (Figure 8A). In the antagonism experiments, the CB1 receptor blocker rimonabant ($\chi^2 = 18.570$, $P < 0.001$), but not the CB2 antagonist, SR144528 ($\chi^2 = 29.829$, $P < 0.001$), blocked the anti-writhing effects of SAR127303 at 3 mg/kg p.o. (Figures 8B and 8C).

The formalin test of inflammatory pain-like behavior in mice. Results of the effects of SAR127303 on pain induced by formalin in mice are shown in Figure 9A and B. In the first experiment, acute treatment with the MAGL inhibitor caused a significant diminution of the late phase [inflammatory phase: AUC (15–45 min): Two-sided Wilcoxon test for factor treatment: $S = 100$, $P < 0.001$], but not the early [nociceptive phase: AUC (0–15 min): $S = 71.5$, $P = 0.75$] phase induced by formalin. In the second experiment, where SAR127303 was administered orally for five consecutive days, a similar suppressive effect was also observed in the late phase [AUC (15–45 min): $S = 97.5$, $P < 0.001$], and again not in the acute phase [AUC (0–15 min): $S = 85$, $P = 0.08$].

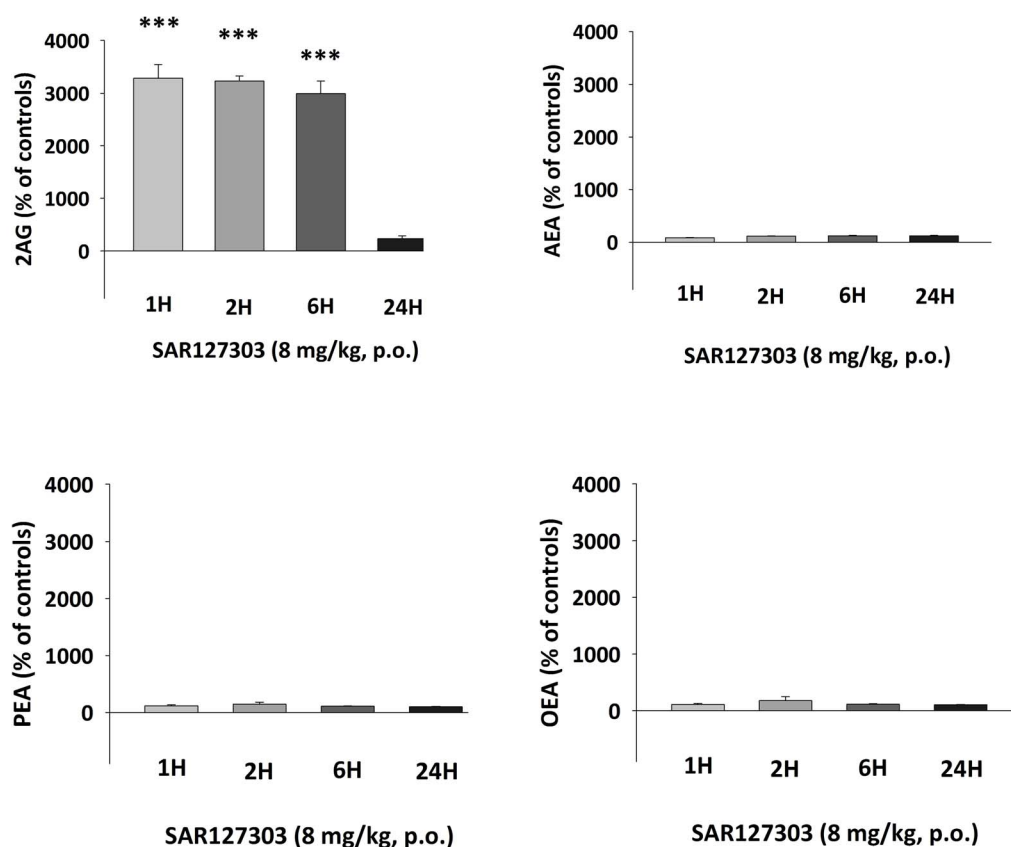


Figure 7 | Levels of 2-AG, AEA, PEA and OEA in the hippocampus of mice treated with 8 mg/kg SAR127303. Data are presented as mean \pm S.E.M.; *** $P < 0.001$ vs baseline level; $N = 3$ per group.

Effects of SAR127303 in models of cognitive processes

In vitro long term potentiation (LTP). In hippocampal slices from vehicle-treated rats, HFS induced a stable LTP, lasting more than 30 minutes. At 1 μM , SAR127303 was found to be completely inactive, while at 10 μM , a slight, albeit non-significant, decrease in LTP amplitude was observed. SAR127303 did not modify baseline fPS amplitude suggesting no effect on basal synaptic transmission (Figure S5).

Effect of 2-AG and SAR127303 on [^3H]ACh release evoked by electrical depolarisation in rat hippocampal slices. 2-AG (10^{-9} , 10^{-8} and 10^{-7} mol/L) (Figure 10A) and SAR127303 (10^{-7} and 10^{-6} mol/L) (Figure 10B) induced a dose-dependent inhibition on [^3H]-ACh release evoked by electrical depolarization in hippocampal slices (-7, -39% and -53% for 2-AG, and -12% and -36% for SAR127303). The effect of 2-AG at 10^{-8} mol/L was completely reversed by the CB1 receptor antagonist, rimonabant (10^{-7} mol/L) (Figure 10C).

Effect of SAR127303 on in vivo hippocampal ACh release in rats. The average level of basal extracellular ACh in the hippocampus (25.25 ± 3.763 pg/40 μL) was defined as the mean of 30 values corresponding to the 10 animals of the experiment and that each represents the mean of the 3 fractions (-40, -20 and 0 minute) before SAR127303 or its vehicle administration. In freely-moving rats, the i.p. administration of SAR127303 induced a global significant decrease of extracellular levels of ACh [$F(1,8) = 10.35$, $P = 0.0123$]. The onset of the decrease was observed immediately after the injection and is significant at 40, 60, 100 and 120 min compared to vehicle treated group (Figure 10D).

The novel object recognition task in mice

Dose-response. Under a protocol in which the two objects were presented one hour following exposure to the familiar object, vehicle-treated animals spent more time exploring the novel one

(17.0 ± 2.2 versus 8.4 ± 1.3 s). The relative time spent exploring the novel object for these animals was significantly above the chance level of fifty (i.e. 65.9 ± 5.4) (Student's t-test: $P = 0.014$) (Fig. 11A). This preferential investigation of the novel object was abolished by administration of 0.125 mg/kg of MK-801 and by SAR127303 at 1 and 10 mg/kg p.o. immediately after presentation of the familiar object. One-way ANOVA indicated a significant treatment effect on novelty index ratio [$F(4,55) = 3.64$, $P < 0.01$]. Further analysis with Dunnett's test showed that MK-801 and SAR127303 at 1 and 10 mg/kg significantly reduced the novelty index ratio as compared to control vehicle. Mice treated with MK-801 or SAR127303 spent the same amount of time investigating both objects.

Antagonism by rimonabant. The same protocol was used as in the dose-response experiment. Similar to this latter, control mice spent a greater amount of time investigating the novel object (Student's t-test: $P = 0.017$), while those treated with 1 mg/kg SAR127303 spent the same amount of time investigating both objects (Fig. 11B). However, when the drug was coadministered with the CB1 receptor antagonist rimonabant at 3 mg/kg, novelty index ratio was significantly different from chance level ($P = 0.026$). It must be noted that ANOVA did not show a significant global effect on novelty index ratio [$F(3,35) = 0.76$, $P = 0.52$].

Repeated treatment. Mice treated with vehicle for 5 days and submitted on day 5 to the same protocol as used in the dose-response experiment, spent again a greater amount of time investigating the novel object (Student's t-test: $P = 0.0003$) (Fig. 11C). Moreover, animals treated with vehicle for 4 days and which received a single administration of SAR127303 at 1 mg/kg on day 5 were unable to discriminate between both objects. Similarly, mice treated repeatedly with SAR127303 at 1 mg/kg p.o. for 5 days failed to discriminate

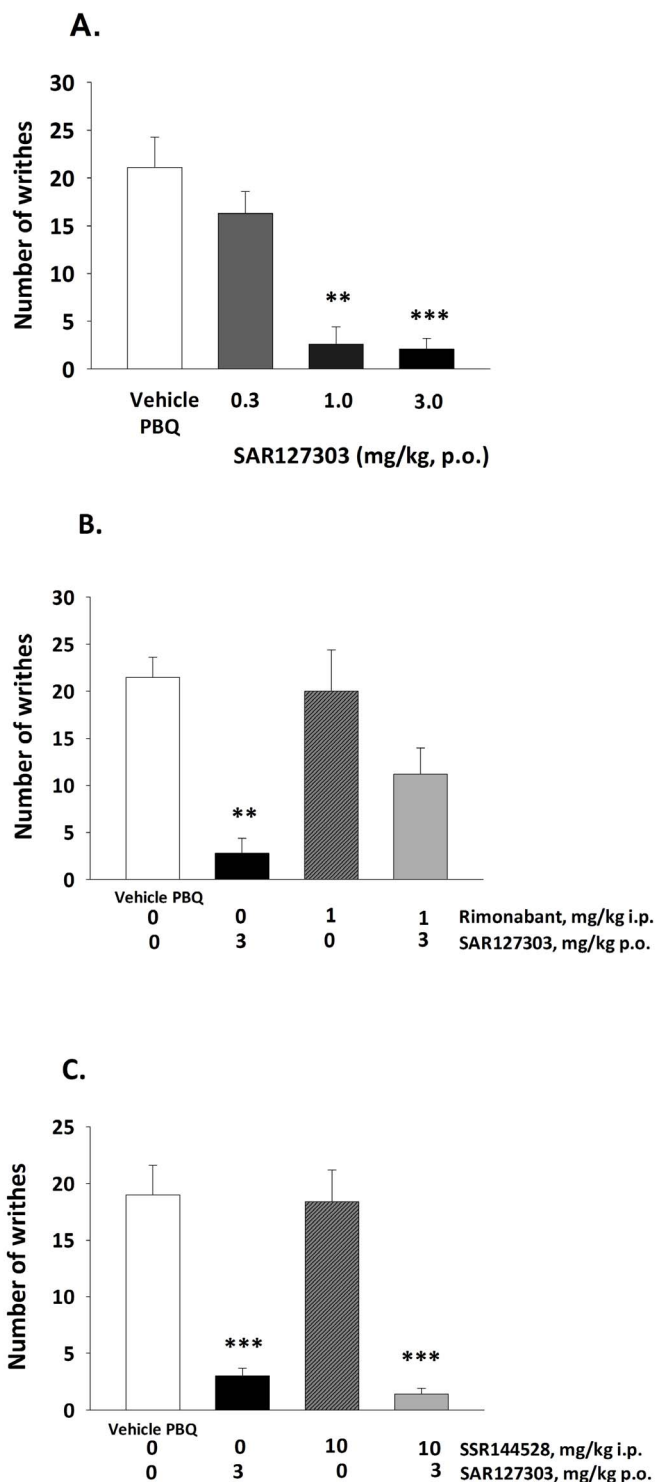


Figure 8 | Effects of SAR127303 alone (A) and in combination with the CB1 receptor antagonist, rimonabant (B), or the CB2 receptor antagonist, SR144528 (C), against writhing induced by phenylbenzoquinone (PBQ) in mice. Each bar represents the average (+ S.E.M) writhes. Post-hoc analyses following Kruskal-Wallis test: ** $P < 0.01$, *** $P < 0.001$ versus vehicle-treated controls. $N = 10$ mice per group.

between the two objects. One-way ANOVA revealed a significant treatment effect on novelty index ratio [$F(2,24) = 3.80$, $P < 0.05$]. Post-hoc analysis using Newman-Keuls test indicated that SAR127303 when given acutely, but not repeatedly, at 1 mg/kg significantly reduced the novelty index ratio as compared to control

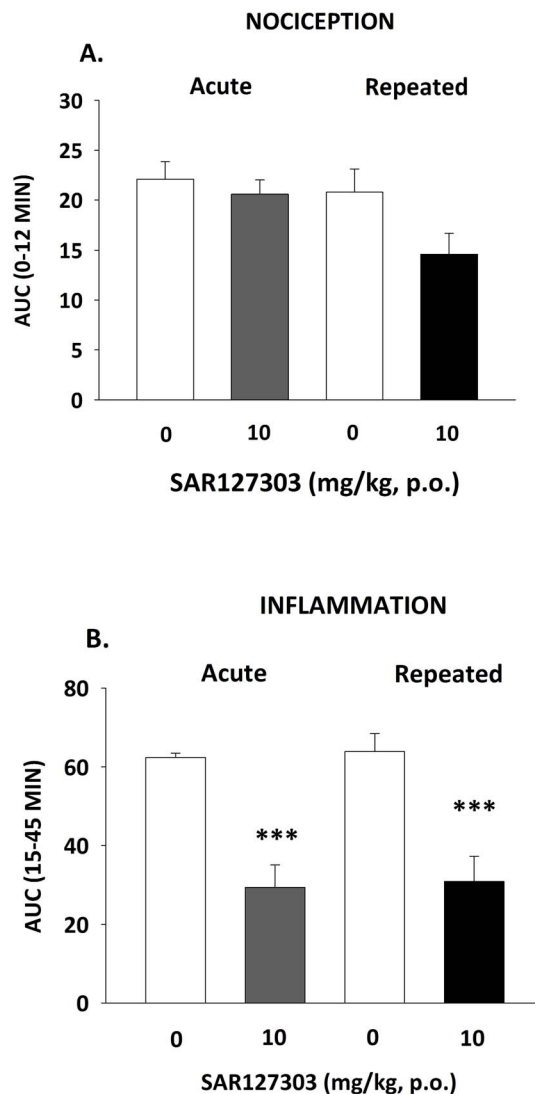


Figure 9 | Effects of acute and repeated (once-a-day for 5 consecutive days) dosing of SAR127303 on formalin-induced pain-like behavior in mice. Each bar represents the average (+ S.E.M.) area under the curve (AUC) of flinching behavior. Two-sided Wilcoxon test for factor treatment: *** $P < 0.001$ versus vehicle-treated controls. $N = 8$ mice per group.

vehicle ($P = 0.037$). However, it must be emphasized that in the repeated treatment group, statistical analysis just failed to reach significance ($P = 0.057$).

The Y-maze test in mice. ANOVA indicated a global significant effect of treatment [$F(4,49) = 6.22$, $P < 0.001$] in the dose-response experiment. Post-hoc Dunnett's *t*-test analysis showed that mice treated with the psychotomimetic PCP (1.5 mg/kg, i.p.) or with SAR127303 at 0.1, 1 and 10 mg/kg, p.o. displayed a significant reduction of spontaneous alternation compared to vehicle-treated mice (Fig. 12). No statistical difference was observed in total number of spontaneous alternation between groups in either experiment (data not shown).

The Morris water maze in rats. Comparison of the data on the first trial at day 1 did not reveal any statistical significance between groups, which would have compromised the interpretation of the learning curves. Two-way ANOVAs indicated a significant treatment effect for all three learning sessions [Day 1: $F(3,36) = 6.35$, $P < 0.01$; Day 2: $F(3,36) = 4.51$, $P < 0.01$; Day 3: $F(3,36) = 5.17$, $P < 0.01$].

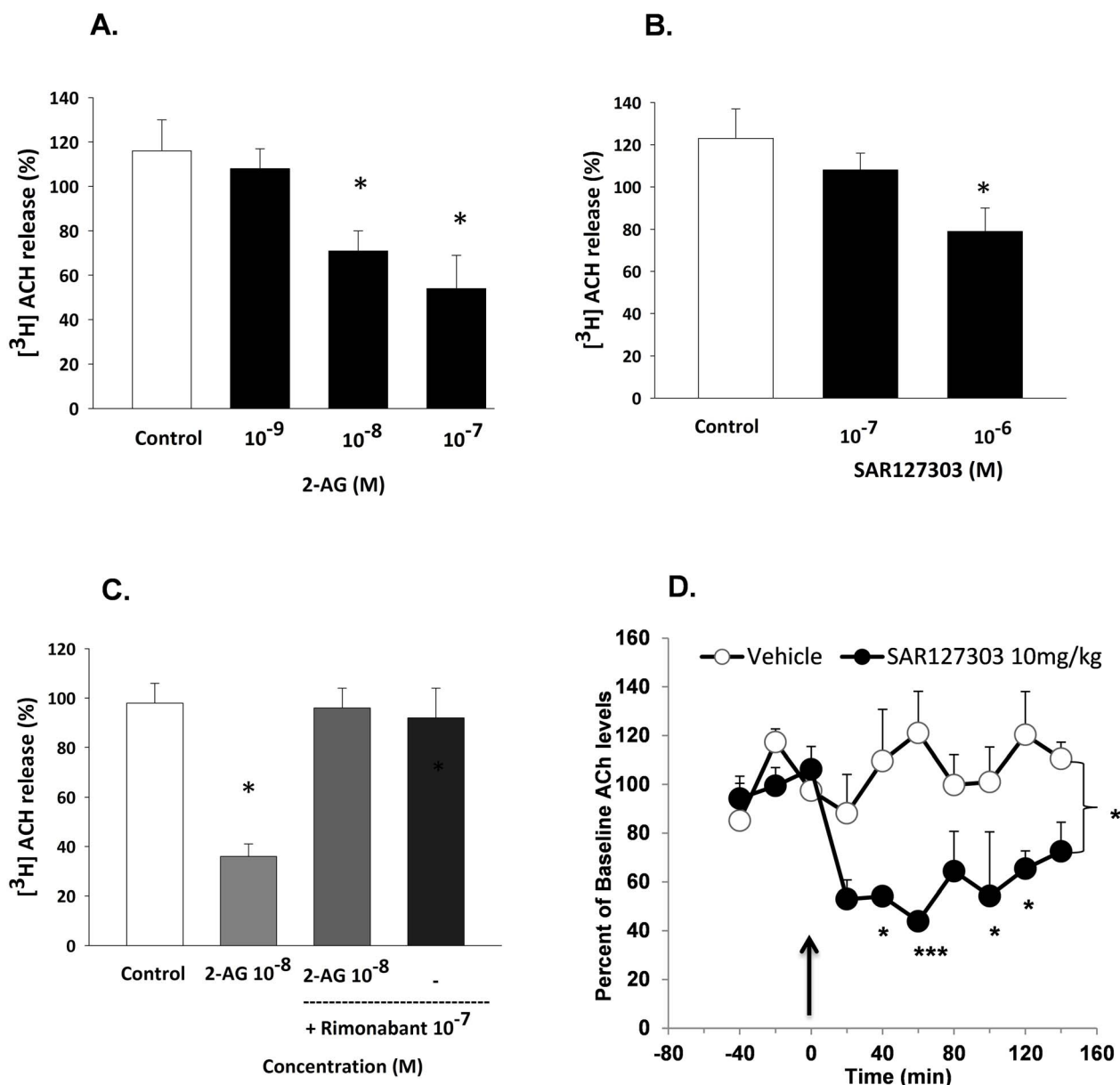


Figure 10 | Effects of 2-AG (A) and SAR127303 (B) on [³H]ACh release evoked by electrical depolarisation in rat hippocampal slices. (C) Blockade by the CB1 receptor antagonist rimobantant of the effects of 2-AG on [³H]ACh release evoked by electrical depolarisation in rat hippocampal slices. Data are expressed as a percentage of basal [³H]-ACh release. * $P < 0.05$ vs control. $N = 3$ slices/group. (D) Effect of SAR127303 on hippocampal ACh release measured by microdialysis in the ventral hippocampus of freely-moving rats. Data are expressed as percent of basal period and are Mean \pm S.E.M. of data. * $P < 0.05$, *** $P < 0.001$. Dunnett's test versus "Vehicle" treated group from 20 to 140 minutes for each level of "Time" with significant global effect of factor "Treatment". $N = 5$ rats/group.

0.01] and a significant inter-trial effects for sessions one [$F(2,72) = 10,65$, $P < 0.0001$] and two [$F(2,72) = 10,20$, $P < 0.001$]. Post-hoc analysis showed that vehicle-treated animals and those that received SAR127303 at 0.1 mg/kg p.o. displayed improved performance at sessions one and two as their latency to reach the platform was decreased significantly over trials (Figure 13). This was in contrast to rats treated with SAR127303 at 10 mg/kg, which failed to improve significantly their performance during the three learning sessions. Similarly, animals from the 1 mg/kg group did not improve significantly their performance at day 1 and 3. However, a significant decrease in latency was observed the second day for trial three. In addition inter-group comparisons showed a significant difference between vehicle-treated animals and rats treated with SAR127303 at 10 mg/kg on day 1 (trials 2 and 3), day 2 (trial 3) and on day 3 (trial 3), and at 1 mg/kg at day 1 (trial 2) (Figure 13).

Effects of SAR127303 in models of seizures. *The 6-Hz electroshock-induced seizures, pentylenetetrazol (PTZ) seizure threshold and kainic acid-induced seizures tests in mice.* SAR127303 was devoid of any protective activity against seizures induced both by 6-Hz stimulation and by the convulsants PTZ and kainic acid (Table S4, supplementary section). This was in contrast to the reference anticonvulsant, levetiracetam ($\chi^2 = 9.7$, $P < 0.01$), and the benzodiazepine, diazepam [$F(2,39) = 59,05$, $P < 0.001$], which afforded full protection in the 6-Hz and PTZ tests, respectively.

The corneal kindling model in mice. Daily treatment with SAR127303 30 mg/kg p.o. delayed the acquisition while decreasing the expression of kindled seizures [$F(16,920) = 5.56$, $P < 0.001$] (Fig. 14A). As compared to the vehicle control group mean seizure severity proved to be significantly lower at all stimulation sessions from day 3. The

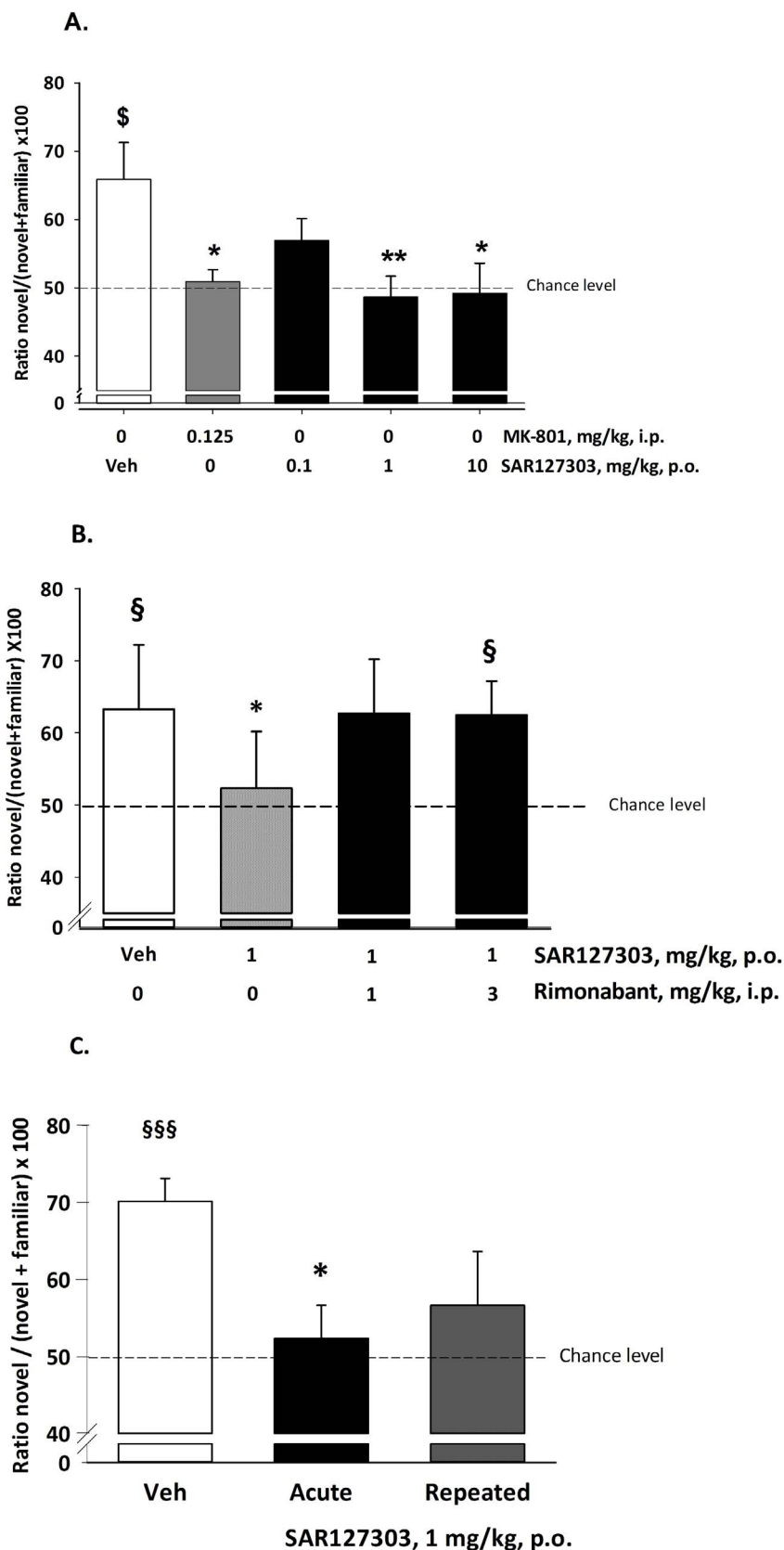


Figure 11 | Effects of oral administration of SAR127303 on short-term visual episodic memory in mice using the novel object recognition test. (A) Dose-response versus the NMDA receptor antagonist MK-801; (B) Antagonism of the effects of SAR127303 by the CB1 receptor antagonist, rimonabant; (C) Comparison of the effects of acute and repeated (5 days, twice-a-day) treatment of SAR127303. Each bar represents the average (+ S.E.M) novelty index ratio. Student's t-test: \$ $P < 0.05$ versus chance level of 50; Post-hoc analyses following one-way ANOVA: * $P < 0.05$, ** $P < 0.01$ versus vehicle-treated controls. $N = 9$ to 13 mice per group.

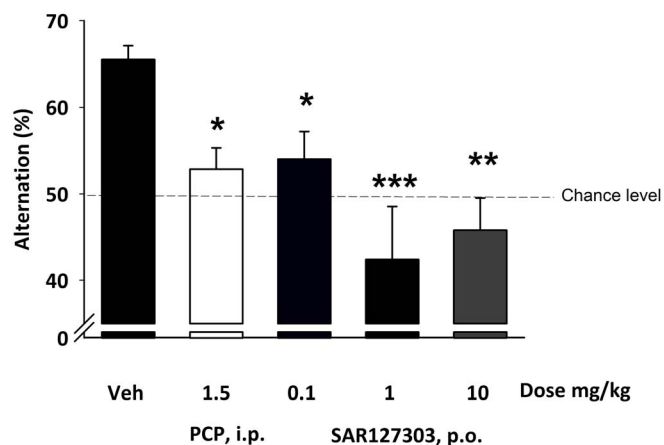


Figure 12 | Effects of oral administration of SAR127303 on spatial working memory in mice using the Y-maze test. (A) Dose-response versus the non-competitive NMDA receptor antagonist, PCP; (B) Antagonism of the effects of SAR127303 by the CB1 receptor antagonist, rimonabant. Bars represent number of arm entries (mean + S.E.M.). Post-hoc analyses following one-way ANOVA: * $P < 0.05$, ** $P < 0.01$, *** $P < 0.001$ versus vehicle-treated controls. $N = 10$ to 12 mice per group.

lowest dosage of SAR127303 used in the present study (10 mg/kg p.o.) produced no significant effect on kindling acquisition. When fully-kindled vehicle-treated mice were treated with 30 mg/kg p.o. SAR127303 on day 11 prior to stimulation, seizure severity proved to be significantly lower as compared to control animals. This effect lasted at least up to 24 h post-dosing [$F(2,36) = 6.49$; $P < 0.01$] (Figure 14B).

Discussion

Enhancing eCB signaling has been considered as a potential strategy to treat several diseases, including affective and neurodegenerative disorders, cancer, gastrointestinal inflammation and pain¹⁰. Preparations based on Δ^9 -tetrahydrocannabinol and its synthetic analogues, which activate directly CB receptors, are used by cancer patients undergoing chemotherapy to increase appetite and decrease nausea, but these compounds produce major central side effects, which seriously limits their use on a routinely basis. However, new generations of endocannabinoid-enhancing compounds that indirectly enhance the functionality of endocannabinoid receptors by inhibiting their catabolism have been discovered. These novel drugs are thought to be more selective and safer than direct agonists based on the assumption that they are active only at sites of on-going production of eCBs¹⁰. Here we describe SAR127303, a highly selective, brain penetrant and orally-active inhibitor of the 2-AG-degrading enzyme, MAGL.

Characterization of the mechanism of action of SAR127303. Our data show that SAR127303 has outstanding selectivity for MAGL in the brain, inhibiting one additional serine hydrolase, ABHD6⁴⁶. Animals treated with SAR127303 display marked and sustained inhibition of MAGL in the absence of effect on FAAH that correlated with ~30-fold elevations in endogenous 2-AG, but not AEA levels in the hippocampus. Comparable inhibitory effects have been observed with recombinant human MAGL. In this latter assay, SAR127303 was 10 times more potent than the reference MAGL inhibitor, JZL184. The increased levels of 2-AG following SAR127303 were maintained for a substantial period of time (≥ 6 hours), but tended to return to baseline by 24 h post-treatment, as did MAGL activity. These observations are consistent with the brain exposure of the inhibitor, which was no longer detected at this time point. To assess whether elevation in 2-AG produced behavioral effects which

are CB1-dependent, we tested SAR127303 in the "tetrad test" for cannabinoid behavior. Our findings show that SAR127303 was completely devoid of such effects up to 30 mg/kg, results which somewhat contrast with those of previous studies showing that MAGL inhibitors produce some cannabimimetic effects in these assays^{29,38,47}. Our protein crystallization data may provide some tentative explanation for these differences. The flexibility of SAR127303 might prevent a full structuration of MAGL, especially the amphipathic helix A4 described as the "anchoring" helix to the cell membrane. This could lead to different localisation of MAGL in brain tissues thus leading to different pharmacological effects.

Characterization of SAR127303 in models of inflammatory pain.

In the rodent skin, spinal cord or peripheral nerves eCB levels can increase following the administration of irritants or inflammatory stimuli (for reviews, see refs. 2,11,48). These modifications have been suggested to be a beneficial response to decrease proinflammatory mediators and re-establishing homeostasis. This idea is substantiated by numerous findings showing that pharmacological inhibition or genetic inactivation of endocannabinoid hydrolysis (targeting MAGL or FAAH) produces antinociceptive effects in a variety of preclinical assays related to inflammatory pain (for recent reviews, refs. 19,49–51). Moreover, both CB1 and CB2 agonists exert antinociceptive and anti-inflammatory actions in these rodent models. The current results are in line with these findings as they show that systemic administration of SAR127303 reduces pain-like behavior in an acute model of inflammatory pain (i.e. formalin) and one model of visceral pain sensation (i.e. phenyl-p-benzoquinone). In the formalin test in mice, these effects were maintained following repeated administration of a dose slightly higher than the lowest dose (i.e. 10 vs 8 mg/kg) producing near-complete inhibition (~90%) of MAGL in this species. This effect is somewhat unexpected considering previous reports describing the effects of MAGL inhibitors (i.e. JZL184 and KML29) in pain assays, which showed that prolonged and almost complete (~80%) inhibition of the enzyme is associated with tolerance to their antinociceptive effects as a probable results of impaired eCB-dependent synaptic plasticity and desensitized brain CB1 receptors^{32,37,38}. It is tempting to suggest that the lack of tolerance to the anti-pain effects of repeated administration of SAR127303 can be explained by its differential impact on synaptic plasticity and CB1 receptors as compared to existing compounds. SAR127303 inhibits both MAGL and ABHD6, a feature not shared by JZL184 and KML29^{29–31}. The α/β hydrolase ABHD6 has been demonstrated to be strategically positioned to regulate neuronal production of 2-AG that reaches pre-synaptic CB1 receptors, while 2-AG at post-synaptic CB1 receptors is thought to be under the control of MAGL^{46,52}. This redundancy has been suggested to provide the eCB system with a greater capacity to control the duration and magnitude of 2-AG signaling. It can be speculated that when both enzymes are simultaneously inhibited, this action may increase and/or prolong the efficacy of 2-AG at CB1 receptors, preventing for example the occurrence of tolerance to the effects of protracted 2-AG hydrolysis blockade. To check this hypothesis it would be interesting to assess the function of the CB1 receptor, using GTP γ S binding for example, to verify if no desensitization occurred under the current experimental conditions. Another possibility would be to use a selective MAGL inhibitor in combination with an ABHD6 inhibitor to determine if there is no functional tolerance following repeated administration. Finally, it would be worth testing the effects of repeated treatment of SAR127303 in other models of inflammatory pain, such as the carrageenan-induced mouse paw oedema test for example, to determine if the lack of tolerance to the anti-inflammatory action of the drug in the formalin test can be generalized to other experimental situations involving inflammatory response.

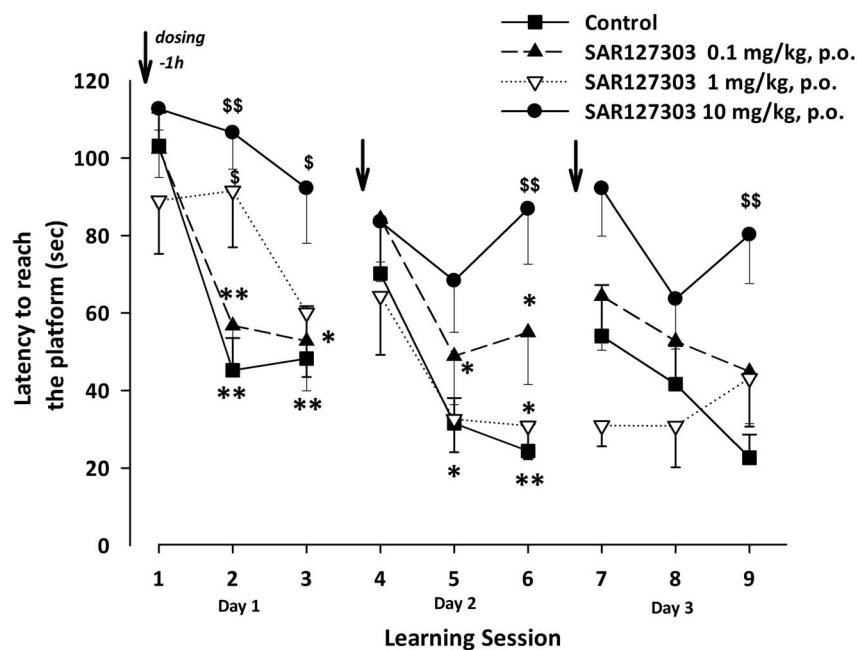


Figure 13 | Effects of oral administration of SAR127303 on spatial reference memory in rats using the Morris water maze. Each line represents the average (\pm S.E.M) latency to reach the platform across trial and learning sessions. Post-hoc analyses following a two-way ANOVA: * $P < 0.05$ and ** $P < 0.01$, vs Trial 1 on each day; \$ $P < 0.05$ and \$\$ $P < 0.01$ vs control-treated rats on each Trial. $N = 10$ rats per group.

Our data further demonstrate that the antinociceptive effects of SAR127303 in the visceral pain model are CB1-, but not CB2-dependent, as demonstrated by the finding that the CB1 antagonist rimonabant, but not the CB2 antagonist SSR144528, blocks this action. These findings agree with previous studies showing that the antinociceptive activity of MAGL inhibitors is mediated by a CB1 receptor mechanism¹⁹. However, the anti-inflammatory pain effects of SAR127303 certainly involve physiological systems and receptor types beyond the CB1 receptor as hypothesized recently by Alhouayek et al.⁵³ who proposed that inflammation involving 2-AG can be mediated by its metabolite arachidonic acid or oxidation of 2-AG by inflammation-induced enzymes such as cyclooxygenase-2 or lipoxygenases, depending the tissue or cellular subtype.

Characterization of SAR127303 in models of learning and memory.

Extensive evidence indicates that eCBs modulate cognitive processes throughout species (for a recent review, see ref. 54). There is general agreement that activation of the eCB system impairs memory acquisition and consolidation. For example, numerous studies have demonstrated that systemic administration of direct (i.e. the CB1 agonists Δ^9 -THC or WIN55,212-2) and indirect (i.e. the FAAH inhibitor, URB597) cannabinoid receptor agonists before or after learning impairs subsequent cognitive performance in a variety of memory assays, such as the MWM, contextual fear conditioning and object recognition in rodents. However, little is known about the cognitive effects of enhanced eCB signalling following selective manipulation of 2-AG. Although in a previous study JZL184 was found to impair MWM performance in mice, it did so only at a dose that also inhibits FAAH (i.e. 40 mg/kg)^{30,33,55}. Here we show that oral administration of SAR127303 over a wide dose-range dramatically impaired acquisition and consolidation in tasks addressing various forms of hippocampal-dependent memory, including spatial, episodic or working memory. Importantly, the memory disruptive effects of MAGL inhibition were blocked by rimonabant, indicating a CB1 receptor mechanism of action. Moreover, repeated administration of SAR127303 did not alter its amnesic action. Pharmacological blockade of MAGL, has been reported to result in dramatic

elevation in brain 2-AG levels⁵⁶, suggesting that selective increase in brain 2-AG levels is associated with memory disruption.

It is likely that at least parts of the cognitive action of SAR127303 is mediated through the activation of hippocampal cannabinoid receptors as a result of the elevation of 2-AG levels produced by the drug. CB1 receptors are highly expressed in hippocampal regions, including the dentate gyrus, CA1, and CA3^{57,58}. Moreover, LTP of CA1 synaptic transmission and hippocampal acetylcholine release, two hallmarks of memory function, were both decreased by SAR127303 in the current study. Interestingly, direct application of 2-AG on rat hippocampal slices inhibits the release of acetylcholine evoked by electrical stimulation in a CB1-dependent manner (current results) and LTP of hippocampal field EPSPs⁵⁹. While the role of other transmitters, such as glutamate or GABA, in the cognitive effects of SAR127303 cannot be excluded, our current data agree with the widely accepted notion that the learning and memory impairments produced by increased eCB signaling is the consequence of a decrease in the release of neurotransmitters below the levels necessary to trigger long-term synaptic modifications which are involved in memory formation⁶⁰.

Characterization of SAR127303 in models of epilepsy.

eCBs have been shown to be increased after the induction of seizures, and synthesized and released on demand to protect against excitotoxic damage through CB1 receptor activation⁶¹. For example, proconvulsant agents such as pilocarpine, kainate or picrotoxin elevate brain levels of AEA or 2-AG when administered to rodents⁶²⁻⁶⁴. These findings prompted speculation that pharmacological modulation of eCB tone might represent a strategy for treating epilepsy. In line with this idea, several reports have demonstrated that eCBs and drugs that increase eCB levels can indeed decrease excitatory vulnerability and seizure susceptibility⁶⁵⁻⁷⁰. These studies used natural and synthetic CB1 receptor agonists or FAAH inhibitors, but none has investigated the effects of selective inhibition of MAGL in animal models for seizures and epilepsy. Here we show that SAR127303 is inactive in the 6-Hz procedure and following the administration of the convulsant PTZ and kainic acid, procedures

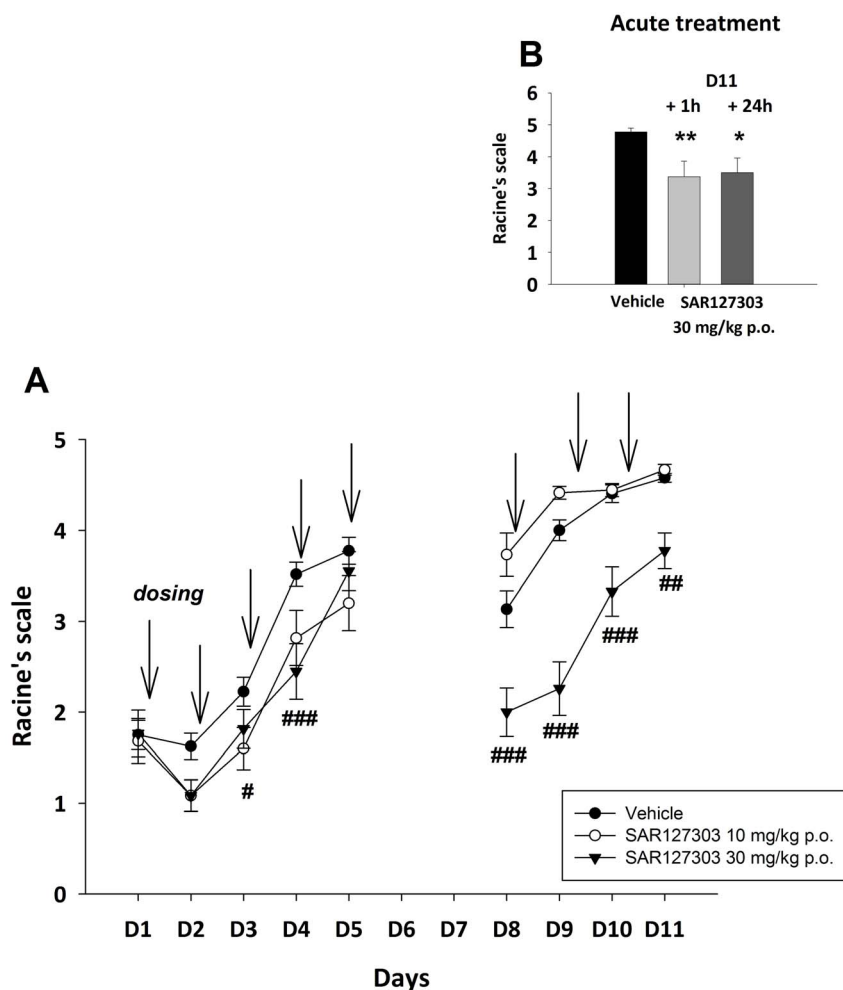


Figure 14 | (A). Effect of different dosages of once daily treatment of SAR127303 on acquisition of kindling, i.e. development of seizure severity upon repeated transcorneal stimulation. Treatment and kindling were interrupted over the weekend on days 6 and 7. (B). Effect of SAR127303 at 30 mg/kg in fully-kindled vehicle-treated mice 11 days after the beginning of kindling. Animals were tested either 60 min or 24 h after drug administration. Data are mean values \pm S.E.M shown for each stimulation session. # $P < 0.05$, ## $P < 0.01$, ### $P < 0.001$, * $P < 0.05$, ** $P < 0.01$ compared to vehicle group. $N = 26$ to 58 mice per group.

claimed to model certain aspects of pharmacoresistant and generalized tonic-clonic seizures in mice⁷¹. This is in contrast to the corneal kindling model of partial epilepsy in mice⁷², where two-week administration of SAR127303 not only delayed the acquisition of kindled seizures, but also decreased their expression. Moreover, in fully kindled animals, a single administration of the drug reduced seizure severity in a long lasting manner as the effect persisted when kindling was continued following wash-out. It is noteworthy that the minimal active dose in the kindling model (30 mg/kg) was higher than those in the pain and cognition models (~1-3 mg/kg), indicating that greater 2-AG hydrolysis inhibition is required to achieve efficacy against seizures. These data indicate that administration of the compound inhibits seizure initiation and protects against focal seizure activity. It can be hypothesized that SAR127303 causes interference with seizure progression by inhibiting propagation of activity from the focus, suggesting that it has the potential to retard the development of epileptogenesis. The mechanisms underlying the neuroprotective action of MAGL blockade remain to be determined. As indicated above, convulsant agents increase brain levels of 2-AG⁷³. It can be hypothesized as was suggested for AEA, that this effect occurs to protect neurons from the effects of altered discharge activity through modulation of calcium and potassium channels, and additional entails a wide range of pro-survival signal transducers via

CB1-dependent events^{61,68,74}. However, to determine if CB1 receptors were involved in the current effects of SAR127303 in the kindling model, additional experiments using CB1 and perhaps CB2 receptor antagonists are warranted. Moreover, the observation that the drug produced these effects at a relatively high dose compared to its effects in the pain and cognition models may indicate the involvement of additional mechanisms, which need to be investigated in future studies.

Conclusion. In conclusion, our study demonstrates that the novel selective and orally-active inhibitor of 2-AG hydrolysis, SAR127303 has anti-inflammatory effects, thus confirming therapeutic potential of MAGL inhibitors against inflammatory pain. Moreover, it provides the first evidence that blockade of 2-AG hydrolysis interferes with the epileptogenesis process and may represent a potential new avenue for the treatment of partial epilepsy. However, our data also reveal that SAR127303 impairs memory performance at a dose-level overlapping with that producing antinociceptive and antiepileptic effects, indicating that MAGL inhibitors are of limited utility as therapeutic agents. Nevertheless, it cannot be ruled out that these compounds may be potentially used to treat diseases associated with the inability to extinguish maladaptive behaviors, such as those for example seen in post-traumatic stress disorder. To verify this idea it would be interesting



in future experiments to assess potential effects of SAR127303 on aversive memory extinction, using for example contextual fear extinction. Moreover, MAGL inhibitors may prove useful in chronic conditions where collateral effects on memory performance may be acceptable (e.g., cancer pain). Finally, the inhibitory properties of SAR127303 of both MAGL and ABHD6, which may explain some of the differences between the current effects and those observed with previous selective MAGL inhibitors deserve further attention.

- Pertwee, R. G. The pharmacology of cannabinoid receptors and their ligands: an overview. *Int. J. Obes. (Lond)* **30 Suppl 1**, S13–S18 (2006).
- Di Marzo, V. & Petrosino, S. Endocannabinoids and the regulation of their levels in health and disease. *Curr. Opin. Lipidol.* **18**, 129–140 (2007).
- Hohmann, A. G. & Suplita, R. L. Endocannabinoid mechanisms of pain modulation. *AAPS. J.* **8**, E693–E708 (2006).
- Jhaveri, M. D., Richardson, D. & Chapman, V. Endocannabinoid metabolism and uptake: novel targets for neuropathic and inflammatory pain. *Br. J. Pharmacol.* **152**, 624–632 (2007).
- Lambert, D. M. Allergic contact dermatitis and the endocannabinoid system: from mechanisms to skin care. *ChemMedChem.* **2**, 1701–1702 (2007).
- Bisogno, T. & Di Marzo, V. Short- and long-term plasticity of the endocannabinoid system in neuropsychiatric and neurological disorders. *Pharmacol. Res.* **56**, 428–442 (2007).
- Matias, I. & Di Marzo, V. Endocannabinoids and the control of energy balance. *Trends Endocrinol. Metab.* **18**, 27–37 (2007).
- Pagotto, U., Marsicano, G., Cota, D., Lutz, B. & Pasquali, R. The emerging role of the endocannabinoid system in endocrine regulation and energy balance. *Endocr. Rev.* **27**, 73–100 (2006).
- Bifulco, M., Laezza, C., Gazerro, P. & Pentimalli, F. Endocannabinoids as emerging suppressors of angiogenesis and tumor invasion (review). *Oncol. Rep.* **17**, 813–816 (2007).
- Di Marzo, V., Bifulco, M. & De, P. L. The endocannabinoid system and its therapeutic exploitation. *Nat. Rev. Drug Discov.* **3**, 771–784 (2004).
- Di Marzo, V. Targeting the endocannabinoid system: to enhance or reduce? *Nat. Rev. Drug Discov.* **7**, 438–455 (2008).
- Piomelli, D. The endocannabinoid system: a drug discovery perspective. *Curr. Opin. Investig. Drugs* **6**, 672–679 (2005).
- Despres, J. P., Golay, A. & Sjostrom, L. Effects of rimonabant on metabolic risk factors in overweight patients with dyslipidemia. *N. Engl. J. Med.* **353**, 2121–2134 (2005).
- Pi-Sunyer, F. X., Aronne, L. J., Heshmati, H. M., Devin, J. & Rosenstock, J. Effect of rimonabant, a cannabinoid-1 receptor blocker, on weight and cardiometabolic risk factors in overweight or obese patients: RIO-North America: a randomized controlled trial. *JAMA* **295**, 761–775 (2006).
- Scheen, A. J., Finer, N., Hollander, P., Jensen, M. D. & Van Gaal, L. F. Efficacy and tolerability of rimonabant in overweight or obese patients with type 2 diabetes: a randomised controlled study. *Lancet* **368**, 1660–1672 (2006).
- Van Gaal, L. F., Rissanen, A. M., Scheen, A. J., Ziegler, O. & Rossner, S. Effects of the cannabinoid-1 receptor blocker rimonabant on weight reduction and cardiovascular risk factors in overweight patients: 1-year experience from the RIO-Europe study. *Lancet* **365**, 1389–1397 (2005).
- Van Gaal, L. F. *et al.* Long-term effect of CB1 blockade with rimonabant on cardiometabolic risk factors: two year results from the RIO-Europe Study. *Eur. Heart J.* **29**, 1761–1771 (2008).
- Moreira, F. A., Griebel, M. & Lutz, B. Central side-effects of therapies based on CB1 cannabinoid receptor agonists and antagonists: focus on anxiety and depression. *Best. Pract. Res. Clin. Endocrinol. Metab.* **23**, 133–144 (2009).
- Fowler, C. J. Monoacylglycerol lipase - a target for drug development? *Br. J. Pharmacol.* **166**, 1568–1585 (2012).
- Gaetani, S., Cuomo, V. & Piomelli, D. Anandamide hydrolysis: a new target for anti-anxiety drugs? *Trends Mol. Med.* **9**, 474–478 (2003).
- Gaetani, S. *et al.* The endocannabinoid system as a target for novel anxiolytic and antidepressant drugs. *Int. Rev. Neurobiol.* **85**, 57–72 (2009).
- Mulvihill, M. M. & Nomura, D. K. Therapeutic potential of monoacylglycerol lipase inhibitors. *Life Sci.* **92**, 492–497 (2013).
- Karlsson, M., Contreras, J. A., Hellman, U., Tornqvist, H. & Holm, C. cDNA cloning, tissue distribution, and identification of the catalytic triad of monoglyceride lipase. Evolutionary relationship to esterases, lysophospholipases, and haloperoxidases. *J. Biol. Chem.* **272**, 27218–27223 (1997).
- Cravatt, B. F. *et al.* Molecular characterization of an enzyme that degrades neuromodulatory fatty-acid amides. *Nature* **384**, 83–87 (1996).
- Bisogno, T. & Maccarrone, M. Latest advances in the discovery of fatty acid amide hydrolase inhibitors. *Expert. Opin. Drug Discov.* **8**, 509–522 (2013).
- Hansen, H. S. Palmitoylethanolamide and other anandamide congeners. Proposed role in the diseased brain. *Exp. Neurol.* **224**, 48–55 (2010).
- De Petrocellis, L. & Di Marzo, V. An introduction to the endocannabinoid system: from the early to the latest concepts. *Best. Pract. Res. Clin. Endocrinol. Metab.* **23**, 1–15 (2009).
- King, A. R. *et al.* Discovery of potent and reversible monoacylglycerol lipase inhibitors. *Chem. Biol.* **16**, 1045–1052 (2009).
- Long, J. Z. *et al.* Selective blockade of 2-arachidonoylglycerol hydrolysis produces cannabinoid behavioral effects. *Nat. Chem. Biol.* **5**, 37–44 (2009).
- Chang, J. W. *et al.* Highly selective inhibitors of monoacylglycerol lipase bearing a reactive group that is bioisosteric with endocannabinoid substrates. *Chem. Biol.* **19**, 579–588 (2012).
- Long, J. Z., Nomura, D. K. & Cravatt, B. F. Characterization of monoacylglycerol lipase inhibition reveals differences in central and peripheral endocannabinoid metabolism. *Chem. Biol.* **16**, 744–753 (2009).
- Schlosburg, J. E. *et al.* Chronic monoacylglycerol lipase blockade causes functional antagonism of the endocannabinoid system. *Nat. Neurosci.* **13**, 1113–1119 (2010).
- Busquets-Garcia, A. *et al.* Differential role of anandamide and 2-arachidonoylglycerol in memory and anxiety-like responses. *Biol. Psychiatry* **70**, 479–486 (2011).
- Sciolino, N. R., Zhou, W., & Hohmann, A. G. Enhancement of endocannabinoid signaling with JZL184, an inhibitor of the 2-arachidonoylglycerol hydrolyzing enzyme monoacylglycerol lipase, produces anxiolytic effects under conditions of high environmental aversiveness in rats. *Pharmacol. Res.* **64**, 226–234 (2011).
- Kinsey, S. G. *et al.* Blockade of endocannabinoid-degrading enzymes attenuates neuropathic pain. *J. Pharmacol. Exp. Ther.* **330**, 902–910 (2009).
- Kinsey, S. G., Naidu, P. S., Cravatt, B. F., Dudley, D. T. & Lichtman, A. H. Fatty acid amide hydrolase blockade attenuates the development of collagen-induced arthritis and related thermal hyperalgesia in mice. *Pharmacol. Biochem. Behav.* **99**, 718–725 (2011).
- Kinsey, S. G. *et al.* Repeated low-dose administration of the monoacylglycerol lipase inhibitor JZL184 retains cannabinoid receptor type 1-mediated antinociceptive and gastroprotective effects. *J. Pharmacol. Exp. Ther.* **345**, 492–501 (2013).
- Ignatowska-Jankowska, B. M. *et al.* In vivo characterization of the highly selective monoacylglycerol lipase inhibitor KML29: Antinociceptive activity without cannabinimetic side effects. *Br. J. Pharmacol.* **229**, 591–601 (2013).
- Bertrand, T. *et al.* Structural basis for human monoglyceride lipase inhibition. *J. Mol. Biol.* **396**, 663–673 (2010).
- Paxinos, G. & Watson, C. *The rat brain: In stereotaxic coordinates* (New York Academic Press, San Diego, 1998).
- Bert, L. *et al.* Rapid and precise method to locate microdialysis probe implantation in the rodent brain. *J. Neurosci. Methods* **140**, 53–57 (2004).
- Damsma, G., Bueren, D. L., Westerink, B. H. C., & Horn, A. S. Determination of acetylcholine and choline in the femtomole range by means of HPLC, a post-column enzyme reactor, and electrochemical detection. *Chromatographia* **24**, 827–831 (1987).
- Ennaceur, A. & Delacour, J. A new one-trial test for neurobiological studies of memory in rats. 1: Behavioral data. *Behav. Brain Res.* **31**, 47–59 (1988).
- Griebel, G. *et al.* SAR110894, a potent histamine H₃-receptor antagonist, displays procognitive effects in rodents. *Pharmacol. Biochem. Behav.* **102**, 203–214 (2012).
- Racine, R. J. Modification of seizure activity by electrical stimulation. I. After-discharge threshold. *Electroencephalogr. Clin. Neurophysiol.* **32**, 269–279 (1972).
- Marrs, W. R. *et al.* The serine hydrolase ABHD6 controls the accumulation and efficacy of 2-AG at cannabinoid receptors. *Nat. Neurosci.* **13**, 951–957 (2010).
- Long, J. Z. *et al.* Dual blockade of FAAH and MAGL identifies behavioral processes regulated by endocannabinoid crosstalk in vivo. *Proc. Natl. Acad. Sci. U. S. A.* **106**, 20270–20275 (2009).
- Ligresti, A., Petrosino, S. & Di, M. V From endocannabinoid profiling to 'endocannabinoid therapeutics'. *Curr. Opin. Chem. Biol.* **13**, 321–331 (2009).
- Piscitelli, F. & Di Marzo, V. "Redundancy" of endocannabinoid inactivation: new challenges and opportunities for pain control. *ACS Chem. Neurosci.* **3**, 356–363 (2012).
- Roques, B. P., Fournie-Zaluski, M. C. & Wurm, M. Inhibiting the breakdown of endogenous opioids and cannabinoids to alleviate pain. *Nat. Rev. Drug Discov.* **11**, 292–310 (2012).
- Salaga, M., Sobczak, M. & Fichna, J. Inhibition of fatty acid amide hydrolase (FAAH) as a novel therapeutic strategy in the treatment of pain and inflammatory diseases in the gastrointestinal tract. *Eur. J. Pharm. Sci.* **52**, 173–179 (2014).
- Savinainen, J. R., Saario, S. M. & Laitinen, J. T. The serine hydrolases MAGL, ABHD6 and ABHD12 as guardians of 2-arachidonoylglycerol signalling through cannabinoid receptors. *Acta Physiol (Oxf)* **204**, 267–276 (2012).
- Alhouayek, M., Masquelier, J. & Muccioli, G. G. Controlling 2-arachidonoylglycerol metabolism as an anti-inflammatory strategy. *Drug Discov. Today* **19**, 295–304 (2013).
- Morena, M. & Campolongo, P. The endocannabinoid system: An emotional buffer in the modulation of memory function. *Neurobiol. Learn. Mem.* **112**, 30–43 (2013).
- Wise, L. E. *et al.* Dual fatty acid amide hydrolase and monoacylglycerol lipase blockade produces THC-like Morris water maze deficits in mice. *ACS Chem. Neurosci.* **3**, 369–378 (2012).
- Chanda, P. K. *et al.* Monoacylglycerol lipase activity is a critical modulator of the tone and integrity of the endocannabinoid system. *Mol. Pharmacol.* **78**, 996–1003 (2010).
- Herkenham, M. *et al.* Cannabinoid receptor localization in brain. *Proc. Natl. Acad. Sci. U. S. A.* **87**, 1932–1936 (1990).



58. Herkenham, M. *et al.* Characterization and localization of cannabinoid receptors in rat brain: a quantitative in vitro autoradiographic study. *J. Neurosci.* **11**, 563–583 (1991).
59. Stella, N., Schweitzer, P. & Piomelli, D. A second endogenous cannabinoid that modulates long-term potentiation. *Nature* **388**, 773–778 (1997).
60. Sullivan, J. M. Cellular and molecular mechanisms underlying learning and memory impairments produced by cannabinoids. *Learn. Mem.* **7**, 132–139 (2000).
61. Marsicano, G. *et al.* CB1 cannabinoid receptors and on-demand defense against excitotoxicity. *Science* **302**, 84–88 (2003).
62. Wallace, M. J., Martin, B. R. & DeLorenzo, R. J. Evidence for a physiological role of endocannabinoids in the modulation of seizure threshold and severity. *Eur. J. Pharmacol.* **452**, 295–301 (2002).
63. Wallace, M. J., Blair, R. E., Falenski, K. W., Martin, B. R. & DeLorenzo, R. J. The endogenous cannabinoid system regulates seizure frequency and duration in a model of temporal lobe epilepsy. *J. Pharmacol. Exp. Ther.* **307**, 129–137 (2003).
64. Solbrig, M. V., Adrian, R., Baratta, J., Piomelli, D. & Giuffrida, A. A role for endocannabinoids in viral-induced dyskinetic and convulsive phenomena. *Exp. Neurol.* **194**, 355–362 (2005).
65. Naderi, N., Aziz, A. F., Shafaghi, B., Najarkolaei, A. H. & Motamedi, F. Evaluation of interactions between cannabinoid compounds and diazepam in electroshock-induced seizure model in mice. *J. Neural Transm.* **115**, 1501–1511 (2008).
66. Naderi, N., Ahmad-Molaei, L., Aziz, A. F. & Motamedi, F. Modulation of anticonvulsant effects of cannabinoid compounds by GABA-A receptor agonist in acute pentylenetetrazole model of seizure in rat. *Neurochem. Res.* **36**, 1520–1525 (2011).
67. Wendt, H., Soerensen, J., Wotjak, C. T. & Potschka, H. Targeting the endocannabinoid system in the amygdala kindling model of temporal lobe epilepsy in mice. *Epilepsia* **52**, e62–e65 (2011).
68. Karanian, D. A. *et al.* Endocannabinoid enhancement protects against kainic acid-induced seizures and associated brain damage. *J. Pharmacol. Exp. Ther.* **322**, 1059–1066 (2007).
69. Vilela, L. R. *et al.* Effects of cannabinoids and endocannabinoid hydrolysis inhibition on pentylenetetrazole-induced seizure and electroencephalographic activity in rats. *Epilepsy Res.* **104**, 195–202 (2013).
70. Citraro, R. *et al.* Antiepileptic action of N-palmitoylethanolamine through CB1 and PPAR-alpha receptor activation in a genetic model of absence epilepsy. *Neuropharmacology* **69**, 115–126 (2013).
71. Löscher, W. Critical review of current animal models of seizures and epilepsy used in the discovery and development of new antiepileptic drugs. *Seizure*. **20**, 359–368 (2011).
72. Matagne, A. & Klitgaard, H. Validation of corneally kindled mice: a sensitive screening model for partial epilepsy in man. *Epilepsy Res.* **31**, 59–71 (1998).
73. Sugiura, T., Yoshinaga, N., Kondo, S., Waku, K. & Ishima, Y. Generation of 2-arachidonoylglycerol, an endogenous cannabinoid receptor ligand, in microtoxinin-administered rat brain. *Biochem. Biophys. Res. Commun.* **271**, 654–658 (2000).
74. Derkinderen, P. *et al.* Regulation of extracellular signal-regulated kinase by cannabinoids in hippocampus. *J. Neurosci.* **23**, 2371–2382 (2003).

Author contributions

G.G. wrote the main manuscript text; P.P., S.B. and T.B. prepared figures; A.J., A.R., B.Z., F.S., F.V., H.A., J.E., J.H., L.B., M.L.G., N.M., N.R., Q.Y., S.B., S.Br., T.B., T.H., T.L., T.T., V.M. carried out experiments; D.F., D.W., F.A., J.E., L.E., M.D., O.E.B., P.A., P.G., P.P., T.B., V.M., V.Mi. reviewed the manuscript.

Additional information

Supplementary information accompanies this paper at <http://www.nature.com/scientificreports>

Competing financial interests: Yes there is potential Competing Interest. Organizations from whom the authors have received compensation for professional services: Guy Griebel, employee of Sanofi; Philippe Pichat, employee of Sanofi; Sandra Beeské, employee of Sanofi; Thibaud Leroy, employee of Sanofi; Nicolas Redon, employee of Sanofi; Agnès Jacquet, employee of Sanofi; Dominique Françon, employee of Sanofi; Lionel Bert, employee of Sanofi; Luc Even, employee of Sanofi; Mati Lopez-Grancha, employee of Sanofi; Tatiana Tolstykh, employee of Sanofi; Fangxian Sun, employee of Sanofi; Qunyan Yu, employee of Sanofi; Scott Brittain, employee of Sanofi; Heike Arlt, employee of Sanofi; Timothy He, employee of Sanofi; Bailin Zhang, employee of Sanofi; Dmitri Wiederschain, employee of Sanofi; Thomas Bertrand, employee of Sanofi; Jacques Houtmann, employee of Sanofi; Alexey Rak, employee of Sanofi; François Vallée, employee of Sanofi; Nadine Michot, employee of Sanofi; Franck Augé, employee of Sanofi; Véronique Menet, employee of Sanofi; Olivier E. Bergis, employee of Sanofi; Pascal George, employee of Sanofi; Patrick Avenet, employee of Sanofi; Vincent Mikol, employee of Sanofi; Michel Didier, employee of Sanofi; Johanna Escoubet, employee of Sanofi.

How to cite this article: Griebel, G. *et al.* Selective blockade of the hydrolysis of the endocannabinoid 2-arachidonoylglycerol impairs learning and memory performance while producing antinociceptive activity in rodents. *Sci. Rep.* **5**, 7642; DOI:10.1038/srep07642 (2015).



This work is licensed under a Creative Commons Attribution-NonCommercial-NoDerivs 4.0 International License. The images or other third party material in this article are included in the article's Creative Commons license, unless indicated otherwise in the credit line; if the material is not included under the Creative Commons license, users will need to obtain permission from the license holder in order to reproduce the material. To view a copy of this license, visit <http://creativecommons.org/licenses/by-nc-nd/4.0/>

SUPPLEMENTARY MATERIAL

Selective blockade of the hydrolysis of the endocannabinoid 2-arachidonoylglycerol impairs learning and memory performance while producing antinociceptive activity in rodents

Guy Griebel, Philippe Pichat, Sandra Beeské, Thibaud Leroy, Nicolas Redon, Agnès Jacquet, Dominique Françon, Lionel Bert, Luc Even, Mati Lopez-Grancha, Tatiana Tolstykh, Fangxian Sun, Qunyan Yu, Scott Brittain, Heike Arlt, Timothy He, Bailin Zhang, Dmitri Wiederschain, Thomas Bertrand, Jacques Houtmann, Alexey Rak, François Vallée, Nadine Michot, Franck Augé, Véronique Menet, Olivier E. Bergis, Pascal George, Patrick Avenet, Vincent Mikol, Michel Didier, Johanna Escoubet

Supplementary Material: The GPCR, ion channel and enzyme panel: Acetylcholinesterase; Adenosine A1, A2A; ATPase (NA⁺/K⁺); α -adrenergic α 1A, α 2A; β -adrenergic β 1, β 2; Cav3.1; cannabinoid CB1, CB2; dopamine D1, D2S; glycine (strychnine-sensitive); histamine H1, H2; hERG; Kv4.3; muscarine M1, M2, M3; MAO-A; nicotine α 4 β 2; serotonin 5-HT1A, 5-HT2A, 5-HT2B; Ca²⁺ channel; K⁺ V channel; SK⁺ Ca channel; Cl⁻ channel (GABA-gated); Nav1.2; Nav1.5; NE transporter; DA transporter; PDE3

Table S1 : The kinase panel

	Kinase Name	Kinase Name (Caliper)	Kinase Name (PKP)	Official Gene Name	Kinase Group	Official Full Name
1	MAPKAP K2	MAPKAPK2	MAPKAP K2	MAPKAPK 2	CAMK	mitogen-activated protein kinase-activated protein kinase 2
2	AurA	AurA	Aurora2	AURKA	Other	aurora kinase A
3	PKCz	PKCz	PKCz	PRKCZ	AGC	protein kinase C, zeta
4	RSK1	RSK1	RSK1	RPS6KA1	AGC	ribosomal protein S6 kinase, 90kDa, polypeptide 1
5	MAPKAP K5	PRAK	PRAK	MAPKAPK 5	CAMK	mitogen-activated protein kinase-activated protein kinase 5
6	Erk1	Erk1	ERK1	MAPK3	CMGC	mitogen-activated protein kinase 3
7	PKD2	PKD2	PRKD2	PRKD2	CAMK	Protein kinase D2
8	CK1d	CK1d	CK1d	CSNK1D	CK1	casein kinase 1, delta
9	CHK1	CHK1	CHK1	CHEK1	CAMK	CHK1 checkpoint homolog (S. pombe)
10	ABL	ABL	ABL1	ABL1	TK	c-abl oncogene 1, receptor tyrosine kinase
11	FYN	FYN	p59FYN	FYN	TK	FYN oncogene related to SRC, FGR, YES
12	LYNa	LYN	LynA	LYN	TK	V-YES Yamaguchi sarcoma viral related oncogene homolog
13	CHK2	CHK2	CHK2	CHEK2	CAMK	CHK2 checkpoint homolog (S. pombe)
14	MET	MET	METK	MET	TK	met proto-oncogene (hepatocyte growth factor receptor)
15	LCK	LCK	LCK	LCK	TK	Lymphocyte-specific protein tyrosine kinase
16	SRC	SRC	SRC	SRC	TK	V-SRC sarcoma (Schmidt-Ruppin A-2) viral oncogene homolog (avian)
17	GSK3b	GSK3b	GSK3b	GSK3B	CMGC	glycogen synthase kinase 3 beta
18	Erk2	Erk2	p42MAPK	MAPK1	CMGC	mitogen-activated protein kinase 1
19	PKACa	PKA	PKA	PRKACA	AGC	protein kinase, cAMP-dependent, catalytic, alpha
20	AKT2	AKT2	AKT2	AKT2	AGC	v-AKT, murine thymoma viral oncogene homolog 2
21	INSR	INSR	INSRK	INSR	TK	insulin receptor
22	p38a	p38a	p38a	MAPK14	CMGC	mitogen-activated protein kinase 14
23	AKT1	AKT1	AKT1	AKT1	AGC	v-AKT, murine thymoma viral oncogene homolog 1
24	MSK1	MSK1	MSK1	RPS6KA5	AGC	Ribosomal protein S6 kinase, 90kDa, polypeptide 5
25	PKCb2	PKCb2	PKCb2	PRKCB	AGC	protein kinase C, beta
26	ROCK2	ROCK2	ROCK2	ROCK2	AGC	Rho-associated, coiled-coil containing protein kinase 2
27	CDK2	CDK2	CDK2-cyclinA	CDK2	CMGC	cyclin-dependent kinase 2
28	MST2	MST2	MST2	STK3	STE	Serine/threonine kinase 3 (STE20 homolog, yeast)
29	PKG1a	PKGa	PKG1a	PRKG1	AGC	protein kinase, cGMP-dependent, type I
30	PAK2	PAK2	PAK2	PAK2	STE	p21 protein (Cdc42/Rac)-activated kinase 2
31	IGF1R	IGF1R	IGF1RK	IGF1R	TK	insulin-like growth factor 1 receptor
32	FGFR1	FGFR1	FLT2	FGFR1	TK	fibroblast growth factor receptor 1
33	MARK1	MARK1	MARK1	MARK1	CAMK	MAP/microtubule affinity-regulating kinase 1
34	CAMK2d	CAMK2	CAMK2D	CAMK2D	CAMK	calcium/calmodulin-dependent protein kinase II delta
35	PIM2	PIM2	PIM2	PIM2	CAMK	Pim-2 oncogene
36	BTK	BTK	BTK	BTK	TK	Bruton agammaglobulinemia tyrosine kinase
37	c-TAK1	c-TAK1	CTAK1	MARK3		MAP/microtubule affinity-regulating kinase 3
38	DYRK1a	DYRK1a	DYRK1A	DYRK1A	CMGC	dual-specificity tyrosine-(Y)-phosphorylation regulated kinase 1A
39	CaMK4	CAMK4	CaMK4	CAMK4	CAMK	calcium/calmodulin-dependent protein kinase IV
40	AMPK α 1/ β 1/ γ 1	AMPK	AMPK	PRKAA1	CAMK	protein kinase, AMP-activated, alpha 1 catalytic subunit
41	FLT3	FLT3	FLT3	FLT3	TK	fms-related tyrosine kinase 3
42	HGK	HGK	HGK	MAP4K4	CMGC	mitogen-activated protein kinase kinase kinase kinase 4
43	KDR	KDR	KDR	KDR	TK	kinase insert domain receptor (a type III receptor tyrosine kinase)
44	Raf1	c-Raf	cRAF	RAF1	TKL	v-raf-1 murine leukemia viral oncogene homolog 1
45	P70S6K	p70S6K	p70S6K	RPS6KB1	AGC	ribosomal protein S6 kinase, 70kDa, polypeptide 1
46	IRAK4	IRAK4	IRAK4	IRAK4	TKL	Interleukin-1 receptor-associated kinase 4
47	SGK	SGK1	SGK	SGK1	AGC	serum/glucocorticoid regulated kinase 1
48	SYK	SYK	SYK	SYK	TK	Spleen tyrosine kinase
49	AurB	AurB	AurB	AURKB	Other	aurora kinase B
50	FGFR2	FGFR2	FGFR2	FGFR2	TK	fibroblast growth factor receptor 2

51	FGFR3	FGFR3	FGFR3	FGFR3	TK	fibroblast growth factor receptor 3
52	ABL Q252H	Abl(Q252H)	ABL1 (Q252H)	ABL Q252H	TK	c-abl oncogene 1, receptor tyrosine kinase
53	AurC	AurC	AurC	AURKC	Other	aurora kinase C
54	FGFR4	FGFR4	FGFR4	FGFR4	TK	fibroblast growth factor receptor 4
55	EGFR	EGFR	EGFR	EGFR	TK	epidermal growth factor receptor (erythroblastic leukemia viral (v-erb-b) oncogene homolog, avian)
56	ABL T315I	Abl(T315I)	ABL1 (T315I)	ABL T315I	TK	c-abl oncogene 1, receptor tyrosine kinase
57	IKK β	IKK-beta	IKKb	IKBKB	Other	Inhibitor of kappa light polypeptide gene enhancer in B-cells, kinase beta
58	MAPKAP K3	MAPKAPK3	MAPKAP K3	MAPKAPK3	CAMK	mitogen-activated protein kinase-activated protein kinase 3
59	P38 β	p38-beta2	p38b2	MAPK11	CMGC	mitogen-activated protein kinase 11
60	TSSK1	TSSK1	TSSK1	TSSK1B	CAMK	testis-specific serine kinase 1B
61	PKG1 β	PKG1-beta	PKG1b	PRKG1	AGC	protein kinase, cGMP-dependent, type I
62	CAMK2 β	CaMKII_beta	CAMK2b	CAMK2B	CAMK	calcium/calmodulin-dependent protein kinase II beta
63	P38 δ	p38-delta	p38d	MAPK13	CMGC	mitogen-activated protein kinase 13
64	TSSK2	TSSK2	TSSK2	TSSK2	CAMK	testis-specific serine kinase 2
65	ABL H396P	Abl(H396P)	ABL1 (H396P)	ABL H396P	TK	c-abl oncogene 1, receptor tyrosine kinase
66	PDGFR α	PDGFR_alpha	PDGFRa	PDGFRA	TK	platelet-derived growth factor receptor, alpha polypeptide
67	FGFR2 N549H	FGFR2(N549H)	FGFR2 (N549H)	FGFR2 N549H	TK	fibroblast growth factor receptor 2
68	HCK	Hck	HCK	HCK	TK	hemopoietic cell kinase
69	FLT3 D835Y	Flt3(D835Y)	FLT3 (D835Y)	FLT3 D835Y	TK	fms-related tyrosine kinase 3
70	FER	Fer	FER	FER	TK	fer (fps/fes related) tyrosine kinase
71	AKT3	AKT3	AKT3	AKT3	AGC	v-AKT, murine thymoma viral oncogene homolog 3
72	CAMK2 γ	CaMKII_gamma	CAMK2g	CAMK2G	CAMK	calcium/calmodulin-dependent protein kinase II gamma
150	MSK2	MSK2	MSK2	RPS6KA4	AGC	ribosomal protein S6 kinase, 90kDa, polypeptide 4
74	P38 γ	p38-gamma	p38g	PEBP1		phosphatidylethanolamine binding protein 1
75	PKD1	PKD1	PKD1	PRKD1	CAMK	protein kinase D1
76	MARK2	MARK2	MARK2	MARK2	CAMK	MAP/microtubule affinity-regulating kinase 2
77	BMX	BMX	BMX	BMX	TK	BMX non-receptor tyrosine kinase
78	CSNK1A1	CSNK1A1	CK1a	CSNK1A1	CK1	casein kinase 1, alpha 1
79	PKD3	PKD3	PKD3	PRKD3	CAMK	Protein kinase D3
80	BRSK1	BRSK1	BRSK1	BRSK1	CAMK	BR serine/threonine kinase 1
81	NEK2	NEK2	NEK2	NEK2		NIMA (never in mitosis gene a)-related kinase 2
82	PIM1	PIM1	PIM1	PIM1	CAMK	Pim-1 oncogene
83	SGK2	SGK2	SGK2	SGK2	AGC	serum/glucocorticoid regulated kinase 2
84	SGK3	SGK3	SGK3	SGK3	AGC	serum/glucocorticoid regulated kinase family, member 3
85	ARG	Arg	ARG	ABL2	TK	v-abl Abelson murine leukemia viral oncogene homolog 2 (arg, Abelson-related gene)
86	DCAMKL2	DCAMKL2	DCAMKL2	DCLK2	CAMK	doublecortin-like kinase 2
87	RSK2	RSK2	RSK2	RPS6KA3	AGC	ribosomal protein S6 kinase, 90kDa, polypeptide 3
88	RSK3	RSK3	RSK3	RPS6KA2	AGC	ribosomal protein S6 kinase, 90kDa, polypeptide 2
89	BRSK2	BRSK2	BRSK2	BRSK2	CAMK	BR serine/threonine kinase 2
90	PKC α	PKC-alpha	PKCa	PRKCA	AGC	protein kinase C, alpha
91	PKC β 1	PKC-beta1	PKCb1	PRKCB	AGC	protein kinase C, beta
92	PKC γ	PKC-gamma	PKCg	PRKCG	AGC	protein kinase C, gamma
93	PKC δ	PKC-delta	PKCd	PRKCD	AGC	protein kinase C, delta
94	PKC ϵ	PKC-epsilon	PKCe	PRKCE	AGC	protein kinase C, epsilon
95	PKC η	PKC-eta	PKCn	PRKCH	AGC	protein kinase C, eta
96	PKC θ	PKC-theta	PKCt	PRKCQ	AGC	protein kinase C, theta
97	EPHA1	EPHA1	EPHA1	EPHA1	TK	EPH receptor A1
98	EPHA2	EPHA2	EPHA2	EPHA2	TK	EPH receptor A2
99	EPHA3	EPHA3	EPHA3	EPHA3	TK	EPH receptor A3
100	EPHA4	EPHA4	EPHA4	EPHA4	TK	EPH receptor A4
101	EPHA5	EPHA5	EPHA5	EPHA5	TK	EPH receptor A5
102	EPHB2	EPHB2	EPHB2	EPHB2	TK	EPH receptor B2

103	EPHB3	EPHB3	EPHB3	EPHB3	TK	EPH receptor B3
104	EPHB4	EPHB4	EPHB4	EPHB4	TK	EPH receptor B4
105	DYRK1b	DYRK1B	DYRK1b	DYRK1B	CMGC	dual-specificity tyrosine-(Y)-phosphorylation regulated kinase 1B
106	LYNB	LYNB	LYNB	LYN	TK	V-YES Yamaguchi sarcoma viral related oncogene homolog
107	GCK	GCK	GCK	MAP4K2	CMGC	mitogen-activated protein kinase kinase kinase kinase 2
108	MINK	MINK	MINK	MINK	STE	misshapen-like kinase 1 (zebrafish)
109	ABL1 E255K	ABL1(E255K)	ABL1 (E255K)	ABL1 E255K	TK	c-abl oncogene 1, receptor tyrosine kinase
110	FGR	FGR	FGR	FGR	TK	Gardner-Rasheed feline sarcoma viral (v-fgr) oncogene homolog
111	MST1	MST1	MST1	STK4	STE	Serine/threonine kinase 4 (STK4)
112	FLT1	FLT1	FLT1	FLT1	TK	fms-related tyrosine kinase 1 (vascular endothelial growth factor/vascular permeability factor receptor)
113	ABL1 Y253F	ABL1(Y253F)	ABL1 (Y253F)	ABL1 Y253F	TK	c-abl oncogene 1, receptor tyrosine kinase
114	Fes	FES	FES	FES	TK	Feline sarcoma oncogene
115	FLT4	FLT4	FLT4	FLT4	TK	fms-related tyrosine kinase 4
116	TEC	TEC	TEC	TEC	TK	tec protein tyrosine kinase
117	ABL1 G250E	ABL1(G250E)	ABL1 (G250E)	ABL1 G250E	TK	c-abl oncogene 1, receptor tyrosine kinase
118	LTK	LTK	LTK	LTK	TK	leukocyte receptor tyrosine kinase
119	FMS	FMS	FMS	CSF1R	TK	colony stimulating factor 1 receptor
120	HER4	HER4	HER4	ERBB4	TK	v-erb-a erythroblastic leukemia viral oncogene homolog 4 (avian)
121	ROCK1	ROCK1	ROCK1	ROCK1	AGC	Rho-associated, coiled-coil containing protein kinase 1
122	PASK	PASK	PASK	PASK	CAMK	PAS domain containing serine/threonine kinase
123	PHKG1	PhKg1	PHKG1	PHKG1	CAMK	phosphorylase kinase, gamma 1 (muscle)
124	Yes	Yes	YES	YES1	TK	v-yes-1 Yamaguchi sarcoma viral oncogene homolog 1
125	PIM3	PIM3	PIM3	PIM3	CAMK	PIM3 oncogene
126	PHKG2	PhKg2	PHKG2	PHKG2	CAMK	Phosphorylase kinase, gamma 2 (testis)
127	DCAMKL1	DCAMKL1	DCAMKL1	DCLK1	CAMK	doublecortin-like kinase 1
128	EGFR T790M	EGFR(T790M)	EGFR (T790M)	EGFR T790M	TK	epidermal growth factor receptor (erythroblastic leukemia viral (v-erb-b) oncogene homolog, avian)
129	DYRK3	DYRK3	DYRK3	DYRK3	CMGC	dual-specificity tyrosine-(Y)-phosphorylation regulated kinase 3
130	DYRK4	DYRK4	DYRK4	DYRK4	CMGC	Dual-specificity tyrosine-(Y)-phosphorylation regulated kinase 4
131	CLK2	CLK2	CLK2	CLK2	CMGC	CDC-like kinase 2, transcript variant phck2
132	MST1R	MST1R	MST1R	MST1R	TK	macrophage stimulating 1 receptor (c-met-related tyrosine kinase)
133	HIPK1	HIPK1	HIPK1	HIPK1	CMGC	homeodomain interacting protein kinase 1
134	HIPK2	HIPK2	HIPK2	HIPK2	CMGC	homeodomain interacting protein kinase 2
135	RSK4	RSK4	RSK4	RPS6KA6	AGC	ribosomal protein S6 kinase, 90kDa, polypeptide 6
136	PDGFR α V561D	PDGFR-alpha(V561D)	PDGFR α (V561D)	PDGFRA V561D	TK	platelet-derived growth factor receptor, alpha polypeptide
137	EPHA8	EPHA8	EPHA8	EPHA8	TK	EPH receptor A8
138	CDK5/p25	CDK5/p25	CDK5p25	CDK5	CMGC	cyclin-dependent kinase 5
139	Blk	BLK	BLK	BLK	TK	B lymphoid tyrosine kinase
140	ALK	ALK	ALK	ALK	TK	anaplastic lymphoma receptor tyrosine kinase
142	PYK2	PYK2	PYK2	PTK2B	TK	PTK2B protein tyrosine kinase 2 beta
143	DAPK1	DAPK1	DAPK1	DAPK1	CAMK	death-associated protein kinase 1
141	CK1 γ 2	Casein kinase 1 γ 2	CK1 γ 2	CSNK1G2	CK1	casein kinase 1, gamma 2
144	FRK	FRK	FRK	FRK	TK	FYN-related kinase
145	JAK2	JAK2	JAK2	JAK2	TK	Janus kinase 2
146	ROS	ROS (ROS1)	ROS	ROS1	TK	c-ros oncogene 1, receptor tyrosine kinase
147	Ret	RET	RET	RET	TK	RET proto-oncogene (multiple endocrine neoplasia)
148	EPHB1	EPHB1	EPHB1	EPHB1	TK	EPH receptor B1
149	FGFR3 K650E	FGFR3 [K650E]	FGFR3 (K650E)	FGFR3 K650E	TK	fibroblast growth factor receptor 3
150	EGFR T790M L858R	EGFR (ErbB1) T790M L858R	EGFR (T790M, L858R)	EGFR T790M L858R	TK	epidermal growth factor receptor (erythroblastic leukemia viral (v-erb-b) oncogene homolog, avian)

151	RET Y791F	RET Y791F	RET (Y791F)	RET Y791F	TK	RET proto-oncogene (multiple endocrine neoplasia)
152	TXK	TXK	TXK	TXK	TK	TXK tyrosine kinase
153	ITK	ITK	ITK	ITK	TK	IL2-inducible T-cell kinase
154	TYRO3	TYRO3	TYRO3	TYRO3	TK	TYRO3 protein tyrosine kinase
155	CaMK2 α	CaMK2a	CaMK2a	CAMK2A	CAMK	calcium/calmodulin-dependent protein kinase II alpha
156	KIT	KIT	KIT	KIT	TK	v-kit Hardy-Zuckerman 4 feline sarcoma viral oncogene homolog
157	TRKC	TRKC (NTRK3)	TRKC	NTRK3	TK	neurotrophic tyrosine kinase, receptor, type 3
158	Mer	Mer	Mer	MERTK	TK	c-mer proto-oncogene tyrosine kinase
159	CK1 γ 3	CK1g3 (CSNK1G3)	CK1g3	CSNK1G3	CK1	casein kinase 1, gamma 3
160	MET M1250T	MET M1250T	MET (M1250T)	MET M1250T	TK	met proto-oncogene (hepatocyte growth factor receptor)
161	AXL	AXL	AXL	AXL	TK	AXL receptor tyrosine kinase
162	MARK4	MARK4	MARK4	MARK4	CAMK	MAP/microtubule affinity-regulating kinase 4
163	MELK	MELK	MELK	MELK	CAMK	maternal embryonic leucine zipper kinase
164	CDK1/Cyc cB1	CDK1/Cyclin B1	CDK1Cyc linB1	CDC2	CMGC	cell division cycle 2, G1 to S and G2 to M
165	KIT T670I	KIT[T670I]	KIT (T670I)	KIT T670I	TK	v-kit Hardy-Zuckerman 4 feline sarcoma viral oncogene homolog
166	AMPK α 2/ β 1/ γ 1	AMPK-alpha2/beta1/gamma1	AMPK α 2b1g1	PRKAA2	CAMK	protein kinase, AMP-activated, alpha 2 catalytic subunit
167	PKC ι	PRKCI (PKC-iota)	PKC ι	PRKCI	AGC	protein kinase C, iota
168	ZIPK	ZIPK (DAPK3)	ZIPK	DAPK3		death-associated protein kinase 3
169	Ret V804L	Ret (V804L)	RET (V804L)	RET V804L	TK	RET proto-oncogene (multiple endocrine neoplasia)
170	SRM	SRM (SRMS)	SRM	SRMS	TK	src-related kinase lacking C-terminal regulatory tyrosine and N-terminal myristylation sites
171	PRKX	PRKX	PRKX	PRKX	AGC	protein kinase, X-linked
172	GSK3 α	GSK3-alpha	GSK3a	GSK3A	CMGC	glycogen synthase kinase 3 alpha
173	FGFR1 V561M	FGFR1 (V561M)	FGFR1 (V561M)	FGFR1 V561M	TK	fibroblast growth factor receptor 1
174	NTRK2	NTRK2 (TRKB)	TRKB	NTRK2	TK	Neurotrophic tyrosine kinase, receptor, type 2
175	p38 α /SAP K2a T106M	p38alpha/SAP K2a (T106M)	p38a (T106M)	MAPK14 T106M	CMGC	mitogen-activated protein kinase 14
176	DDR2	DDR2	DDR2	DDR2	TK	discoidin domain receptor tyrosine kinase 2
177	CK1 ϵ	CK1-epsilon	CK1e	CSNK1E	CK1	casein kinase 1, epsilon
178	MST3	MST3 (STK24)	MST3	STK24	STE	Serine/threonine kinase 24 (STE20 homolog, yeast)
179	PDGFR α D842V	PDGFRA (D842V)	PDGFRa (D842V)	PDGFRA D842V	TK	platelet-derived growth factor receptor, alpha polypeptide
180	NuaK1	NuaK1	NuaK1	NUAK1	CAMK	NUAK family, SNF1-like kinase, 1
181	CK1 γ 1	CK1-gamma1	CK1g1	CSNK1G1	CK1	casein kinase 1, gamma 1
182	NEK1	NEK1	NEK1	NEK1	Other	NIMA (never in mitosis gene a)-related kinase 1
183	PDGFR β	PDGFR beta	PDGFRb	PDGFRB	TK	platelet-derived growth factor receptor, beta polypeptide
184	MNK1	MNK1 (MKNK1)	MNK1	MKNK1	CAMK	MAP kinase-interacting serine/threonine kinase 1
185	PAK4	PAK4	PAK4	PAK4	STE	p21 protein (Cdc42/Rac)-activated kinase 4
186	CaMK1 α	CaMK1a	CaMK1a	CAMK1	CAMK	calcium/calmodulin-dependent protein kinase I
187	PAK3	PAK3	PAK3	PAK3	STE	p21 protein (Cdc42/Rac)-activated kinase 3
188	IKK ϵ	IKBKE (IKK epsilon)	IKK ϵ	IKBKE	Other	Inhibitor of kappa light polypeptide gene enhancer in B-cells, kinase epsilon
189	PAK5	PAK5 (PAK7)	PAK5	PAK7	STE	p21 protein (Cdc42/Rac)-activated kinase 7
190	CaMK1 δ	CamK1d	CaMK1d	CAMK1D	CAMK	calcium/calmodulin-dependent protein kinase ID
191	LOK	LOK	LOK	STK10	STE	serine/threonine kinase 10
192	CDK3	CDK3	CDK3	CDK3	CMGC	cyclin-dependent kinase 3

Table S2: The pharmacokinetic parameters of SAR127303 in brain and plasma after a single dose of 10 and 30 mg/kg p.o..

Dose mg/kg, p.o.	Tissue	C_{max} ng/mL	T_{max}	AUC_(0-Tlast) ng.h/mL	T_{last} h
10	Plasma	218	4.0	1110	8.0
30		1780	4.0	15500	24
10	Brain	2330	4.0	11200	8.0
30		11100	4.0	123000	24

^aAUC_(0-Tlast), area under the time-concentration curve (measured between 0 and last sampling time, T_{last}); ^bC_{max}, maximal concentration; ^ct_{max}, time required

Table S3: Crystal parameters and data collection statistics are derived from SCALA (Winn et al. 2011). Refinement statistics were obtained from BUSTER-TNT (Vonrhein et al. 2011). Data in parentheses correspond to the highest resolution shells. To calculate R_{free} , 10% of the reflections were excluded from the refinement. R_{sym} is defined as $R_{\text{sym}} = \frac{\sum_{hkl} \sum_i |I_i(hkl) - \langle I(hkl) \rangle|}{\sum_{hkl} \sum_i I_i(hkl)}$.

Data Collection	SAR127303
Wavelength (Å)	0.98140
Resolution (Å)	73.32-2.36
Space group	I222
Unit-cell parameters (Å)	86.2 126.3 138.6
Total reflections	137,665
Total unique reflections	29,609
Rsym	6.0 (45.3)
Completeness (%)	95.2 (97.1)
Mean (I/σ(I))	17.7 (2.6)
Redundancy	4.6 (4.7)
<hr/>	
Refinement statistics	
Rcryst	0.209
Rfree	0.259
<i>Number of reflections</i>	
Total	29,604
Rfree	2,986
<i>Model geometry</i>	
R.m.s.d bonds (Å)	0.002
R.m.s.d angles (°)	0.600
<i>Ramachandran distribution</i>	
Most favored (%)	96.1
Additionally allowed (%)	3.4
Generously allowed (%)	0.5

R.m.s.d, root mean square deviation.

Table S4: Effects of SAR127303 in the 6-Hz electroshock-induced seizures and pentylenetetrazol (PTZ) seizure threshold tests in mice: comparison with the anticonvulsant levetiracetam or the benzodiazepine diazepam

6-Hz electroshock-induced seizures	Seizure severity based on Racine's scale
Vehicle control	4.3±0.1
Levetiracetam 20 mg/kg i.p.	2.7±0.5**
SAR127303 30 mg/kg p.o.	3.6±0.4
Pentylenetetrazol (PTZ) seizure threshold	Convulsant dose (mg/kg PTZ)
Vehicle control	43.8±1.2
Diazepam 3 mg/kg i.p.	81.5±5.33***
SAR127303 30 mg/kg p.o.	38.4±0.95
Kainic acid-induced seizures	Seizure severity based on Racine's scale
Vehicle control	3.2±0.3
SAR127303 30 mg/kg p.o.	3.9±0.3

Data represent mean±S.E.M. ** P<0.01 versus Vehicle control (Kruskal-Wallis), *** P<0.001 versus Vehicle control (Dunnett's test). N = 13 to 16 mice per group.

Reference List

1. Vonrhein C, Flensburg C, Keller P, Sharff A, Smart O, Paciorek W, *et al.* (2011). Data processing and analysis with the autoPROC toolbox. *Acta Crystallogr D Biol Crystallogr* **67**: 293-302.
2. Winn MD, Ballard CC, Cowtan KD, Dodson EJ, Emsley P, Evans PR, *et al.* (2011). Overview of the CCP4 suite and current developments. *Acta Crystallogr D Biol Crystallogr* **67**: 235-242.

Supplement figures

Enzyme activity [1μM]

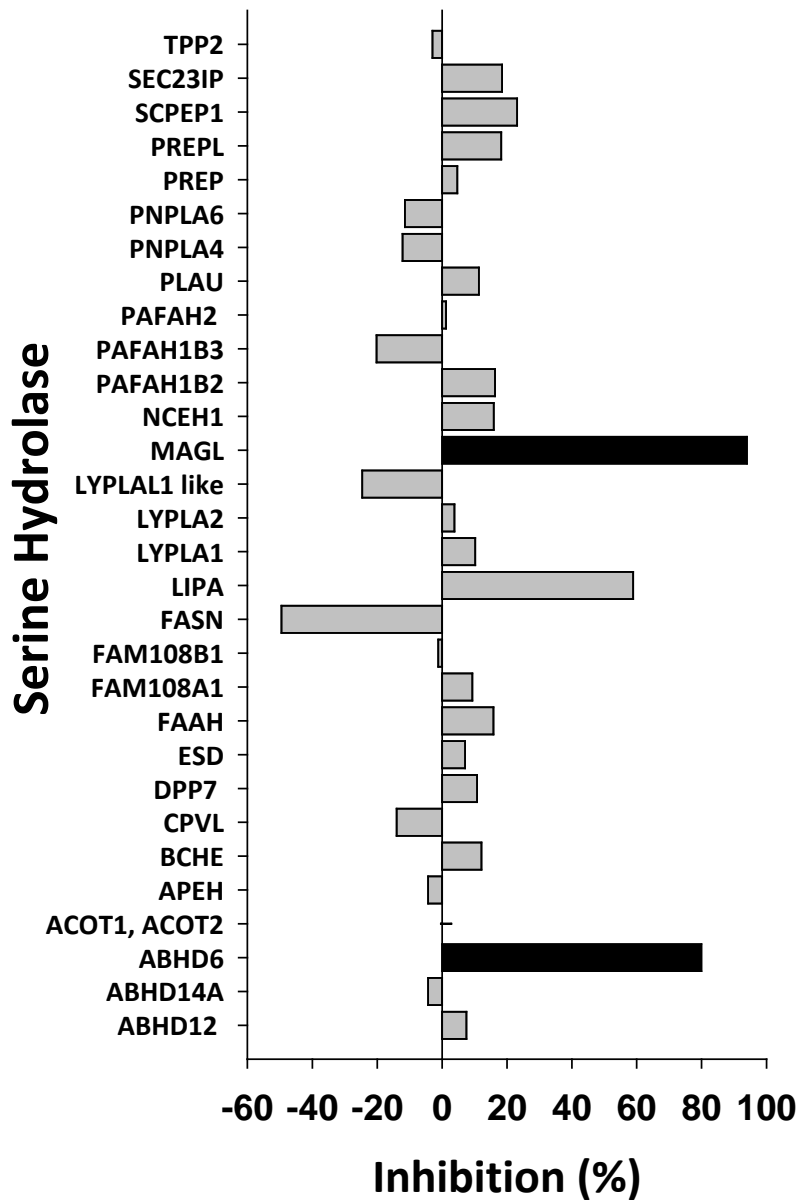


Figure S1: Analysis of serine hydrolases. SAR127303 activity against a panel of serine hydrolases as determined by ActivX Biosciences. Percent inhibition versus DMSO control is shown. TPP2, tripeptidyl-peptidase 2 ; SEC23IP, Sec23p-interacting protein; SCPEP1, Serine carboxypeptidase 1; PREPL, prolyl endopeptidase-like; PREP, prolyl endopeptidase; PNPLA6, patatin-like phospholipase domain containing 6; PNPLA4, patatin-like phospholipase domain containing 4; PLAU, plasminogen activator, urokinase; PAFAH2, platelet-activating factor acetylhydrolase 2; PAFAH1B3, platelet-activating factor acetylhydrolase 1b, catalytic subunit 3; PAFAH1B2, platelet-activating factor acetylhydrolase 1b, catalytic subunit 2; NCEH1, neutral cholesterol ester hydrolase 1; MAGL, monoacylglycerol lipase; LYPLAL1 like, lysophospholipase-like 1; LYPLA2, lysophospholipase II; LYPLA1, lysophospholipase I; LIPA, lipase A; FASN, fatty acid synthase; FAM108B1, abhydrolase domain containing 17B; FAM108A1, abhydrolase domain containing 17A; FAAH, fatty acid amide hydrolase; ESD, esterase D; DPP7, dipeptidyl-peptidase 7; CPVL, carboxypeptidase, vitellogenic-like; BCHE, butyrylcholinesterase; APEH, acylaminoacyl-peptide hydrolase; ACOT1, acyl-CoA thioesterase 1; ACOT2, acyl-CoA thioesterase 2; ABHD6, abhydrolase domain containing 6; ABHD14A, abhydrolase domain containing 14A; ABHD12, abhydrolase domain containing 12.

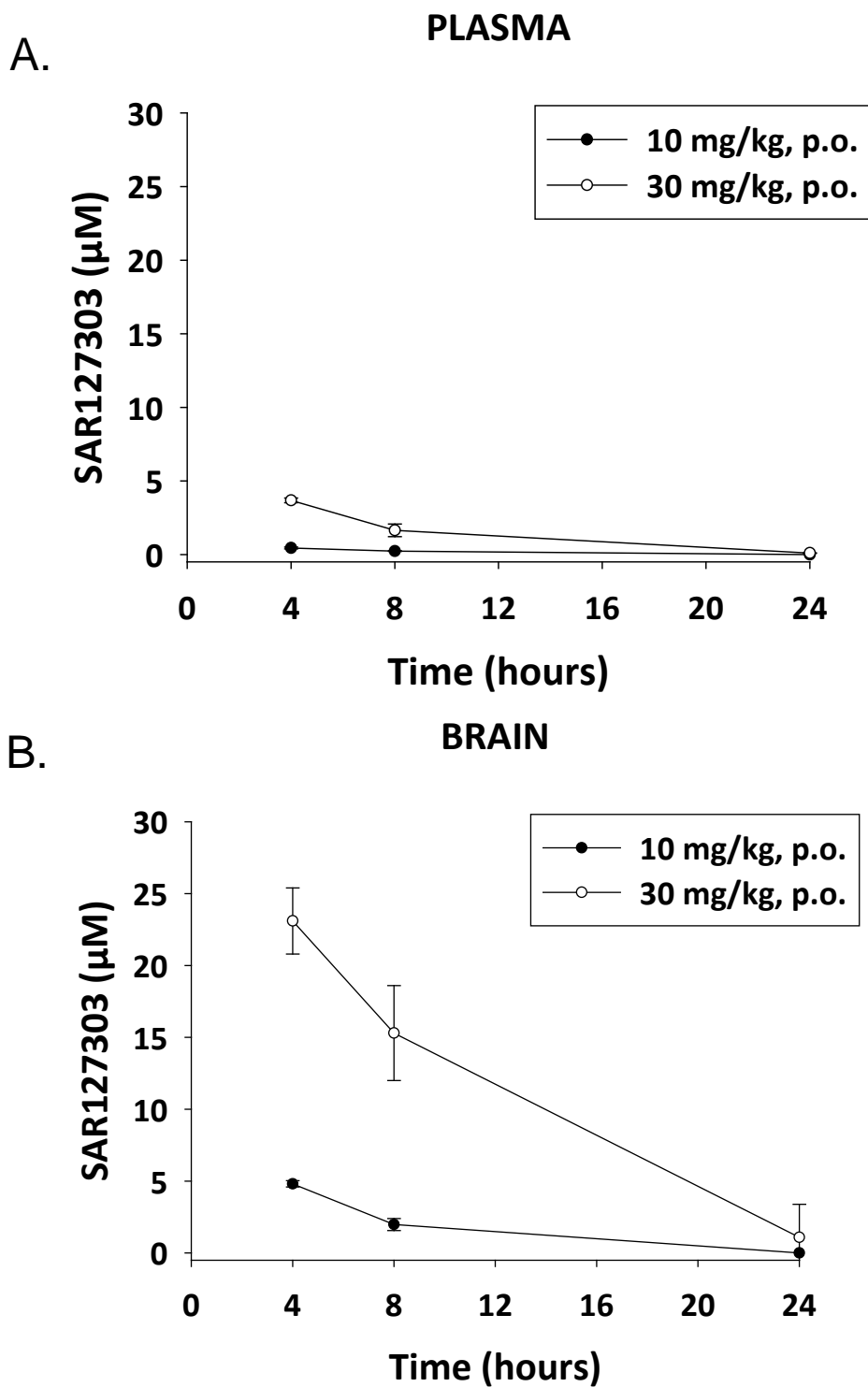
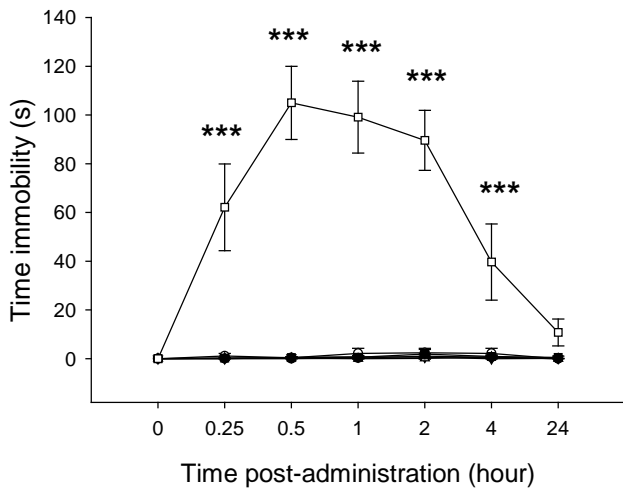
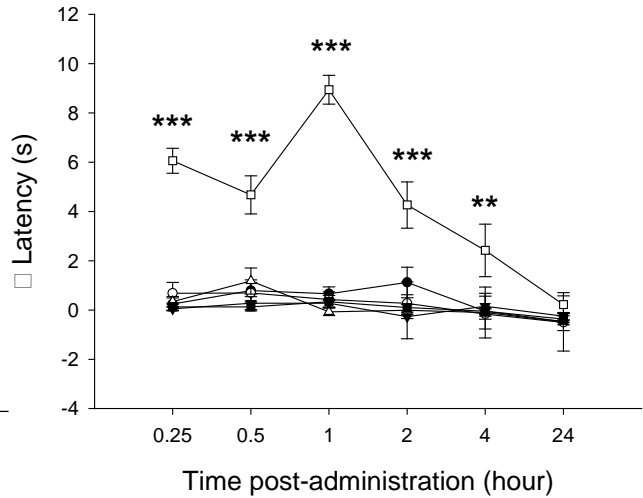


Figure S2: Plasma (A) and brain (B) levels ($\mu\text{M} \pm \text{S.E.M.}$) of SAR127303 as a function of time; $N = 3/\text{time-point}$ for both doses.

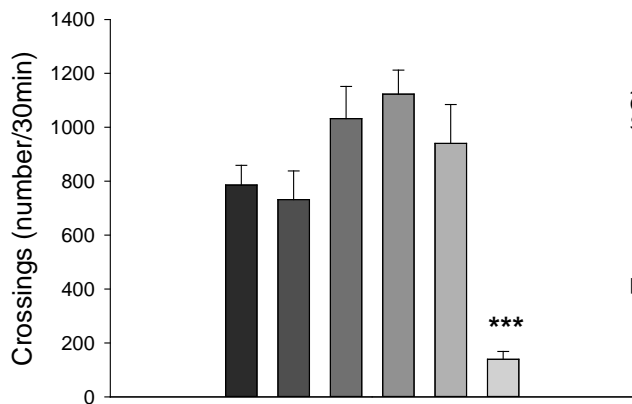
CATALEPSY



TAIL-FLICK



LOCOMOTOR ACTIVITY



RECTAL TEMPERATURE

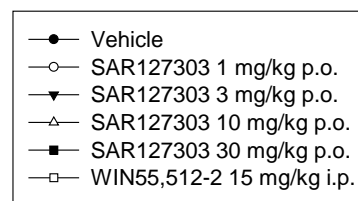
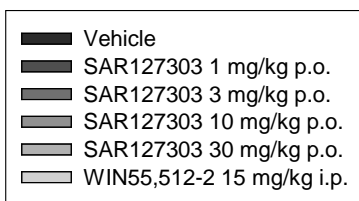
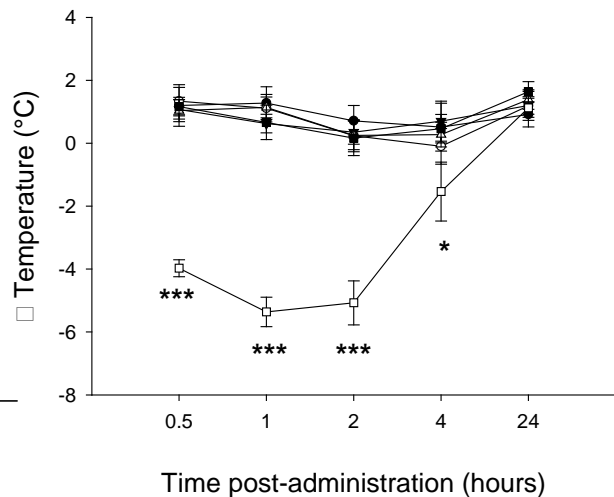


Figure S3: Comparison of the effects of SAR127303 and the CB1 receptor agonist WIN55,512-2 in the tetrad test for cannabinoid behavior. Data represent mean±S.E.M. Post-hoc analyses following one- (locomotor activity) or two- (catalepsy, tail-flick and rectal temperature) way ANOVA: * P<0.05, ** P<0.01, *** P<0.001 versus vehicle-treated controls. N = 8 to 11 mice per group.

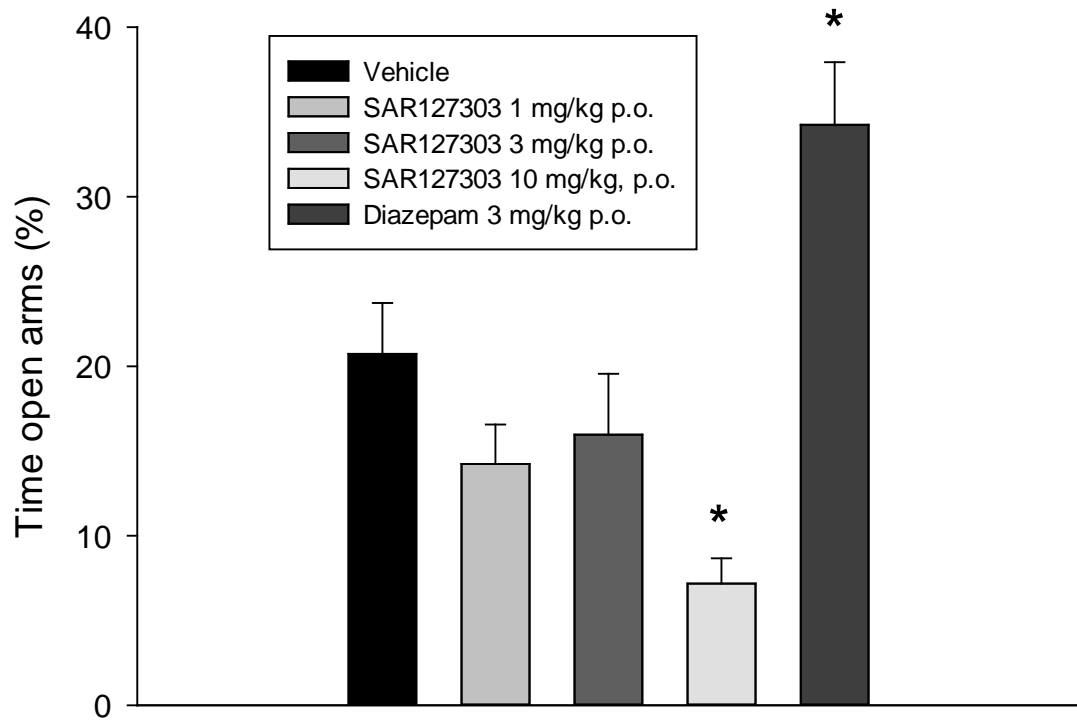


Figure S4: Effects of diazepam and SAR127303 on the behavior of mice on the elevated plus-maze. Bars represent percentage of open arm entries (mean+S.E.M.). Post-hoc analyses following one-way ANOVA: * $P < 0.05$, versus vehicle-treated controls. $N = 12$ mice per group.

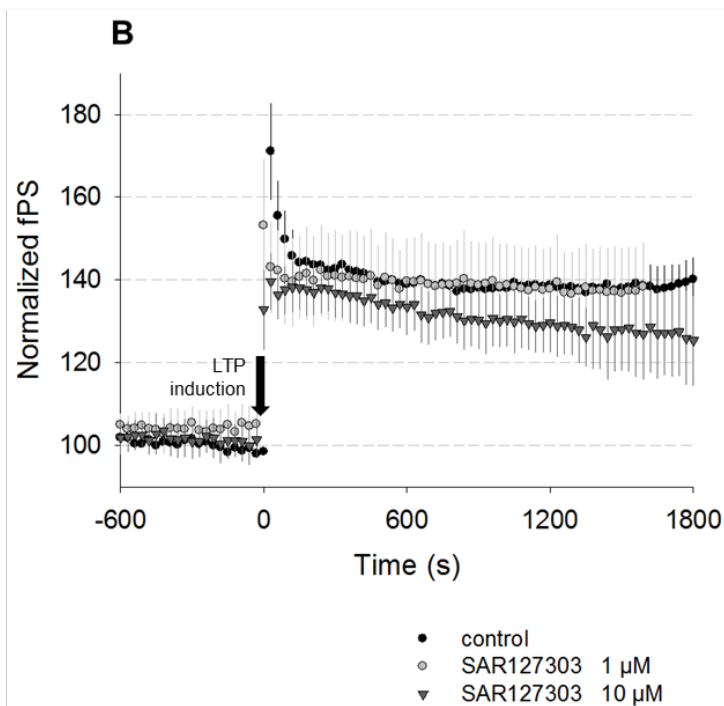
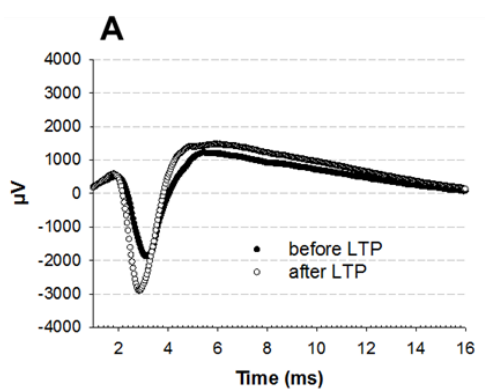


Figure S5: Effects of SAR127303 on LTP in CA1 area of rat hippocampal slices. (A) Typical field population spikes (fPS) time-course recorded from a single electrode 10 min before and 30 min after LTP induction in control condition. (B) Normalized fPS values are plotted as a function of time and superimposed for comparison between control conditions (black circle, average \pm S.E.M, 5 slices) and SAR127303 (1 μ M, gray circle, average \pm S.E.M, 3 slices and 10 μ M, dark gray triangle, average \pm S.E.M, 3 slices).